Chemical tools to modulate endocannabinoid biosynthesis

Deng, H.

3

Rapid and profound rewiring of brain lipid signaling networks by acute diacylglycerol lipase inhibition

Based on
H. Deng, D. Ogasawara, A. Viader, M. P. Baggelaar, A. Breman, H. den Dulk, A. M. C. H. van den Nieuwendijk, M. Soethoudt, T. van der Wel, J. Zhou, H. S. Overkleeft, M. Sanchez-Alavez, S. Mori, W. Nguyen, B. Conti, X.J. Liu, Y. Chen, Q.S. Liu, B. F. Cravatt, M. van der Stelt, *Proc. Natl. Acad. Sci. USA*, **2016**, 113, 26-33.

Introduction

Classically understood forms of neurotransmission involve polar small molecules that are stored in synaptic vesicles and released in response to depolarizing signals that promote vesicle fusion with the presynaptic plasma membrane of neurons.[1] More recently, lipids have emerged as a distinct type of chemical messenger in the nervous system that appear to be generated at the time of their intended action rather than amassed in vesicles.[2-5] This “on-demand” model for production implicates lipid biosynthetic enzymes as major regulators of chemical signaling in the central nervous system (CNS). In support of this premise, the enzymes that produce several classes of lipid transmitters, including lysophospholipids,[6] eicosanoids,[7] and endocannabinoids[8,9] are highly expressed in the nervous system and play important roles in brain development, synaptic plasticity, and the modulation of complex

behaviors. The diacylglycerol (DAG) lipase enzymes DAGLα and DAGLβ,[10] for instance, produce the endocannabinoid 2-arachidonoylglycerol (2-AG),[11,12] and the constitutive genetic disruption of DAGLα lowers brain 2-AG and arachidonic acid content,[13,14] resulting in impaired synaptic plasticity,[13,14] hypophagia,[15] enhanced anxiety and fear responses,[16,17] and propensity for spontaneous seizures.[15]

Many bioactive lipids share structural features and can be, in principle, connected to one another through multi-step metabolic routes,[2,18,19] suggesting the potential for crosstalk among lipid signaling pathways *in vivo*. Such crosstalk could produce more sophisticated forms of integrated or counter-balanced signal transduction to affect complex physiological or disease processes in a dynamic manner. The extent to which individual enzymes within larger metabolic pathways exert control over a multitude of bioactive lipids, however, remains poorly understood. This question can be studied in genetically modified mice lacking specific lipid metabolic enzymes, but the long-term, constitutive inactivation of enzymes renders these models poorly suited for distinguishing rapid and dynamic processes from slower, adaptive changes that may occur in lipid pathways. Pharmacological approaches, on the other hand, provide a powerful means to assess the temporal consequences of acute enzyme blockade on the dynamic composition of lipid networks in the brain under both physiological and pathological conditions. Unfortunately, selective and *in vivo*-active inhibitors are not yet available for many lipid biosynthetic enzymes. Known inhibitors for DAGLs, for instance, have been used to study the function of 2-AG as a retrograde messenger in neuronal cell and/or brain slice preparations,[20-25] but these inhibitors lack the selectivity,[26] potency, and/or chemical properties[21] required for central activity *in vivo*.

In Chapter 2, DH376 was described as a potent and selective, covalent 1,2,3-triazole urea inhibitor for DAGLα and DAGLβ, which provides an excellent chemical tool for investigating DAGL function *in vivo*. This Chapter presents data revealing that acute pharmacological blockade of DAGL by using DH376 and its analogue DO34 leads to a rapid and dramatic reorganization of lipid signaling pathways in the brain that includes elevations in bioactive DAGs and reductions in the two major endocannabinoids, 2-arachidonoylglycerol (2-AG) and *N*-arachidonoylethanolamine (anandamide or AEA), arachidonic acid, and the prostaglandins PGD_2 and PGE_2. The DAGL inhibitors also impaired endocannabinoid-dependent forms of synaptic plasticity and attenuated lipopolysaccharide-induced neuroinflammatory responses, including reductions in core body temperature (anapyrexia). These findings highlight the special role that DAGL enzymes play as integrative nodes for coordinating crosstalk among several classes of lipid transmitters to modulate neuro(immuno)logical functions in the CNS.

Results and Discussion

Potent and selective 1,2,3-triazole ureas inhibitors of DAGLα

The development of DAGL inhibitors has been historically hindered by a dearth of assays for monitoring the activity of these enzymes in native biological systems. Recently tailored activity-based probes were introduced that enable the independent and concurrent monitoring of DAGLα and DAGLβ activities in brain and other tissue/cell types.[27,28] Guided by competitive activity-based protein profiling (ABPP) methods,[29] one of these tailored probes was converted into a series of potent 1,4-substituted, 1,2,3-triazole urea (1,2,3-TU) inhibitors of DAGLβ that displayed peripheral, but not central activity *in vivo*[27] (e.g., KT172 (**1**), Figure 1a). Further modification and optimization of the 1,2,3-TU scaffold was performed to generate selective and CNS-active inhibitors of DAGLα and β. In brief, modifications to the distal phenyl ring appended to the triazole leaving group of KT172 yielded inhibitors with good potency for DAGLα and moderate inhibition of DAGLβ, but the resulting compounds showed little or no CNS activity *in vivo*. Therefore, attention was turned to modifying the staying group of the 1,2,3-TU scaffold (Figure 1a, blue). This, in combination with truncated variations of the triazole leaving group (Figure 1a, black), furnished DO34, a structural analog distinct from DH376 (See Chapter 2), which was identified as a highly potent DAGL inhibitor (Figure 1a). Both DH376 and DO34 blocked the DAGLα conversion of 1-stearoyl-2-arachidonoyl-*sn*-glycerol (SAG) to 2-AG with IC_{50} values of 7 nM (2–26 nM; 95% CI, n=4) and 27 nM (7-98 nM; 95% CI, n=4), respectively (Figure 1b and Table 1), as determined using a real-time, fluorescence-based natural substrate assay with membrane lysates from HEK293T cells expressing recombinant human DAGLα.[30] Using this substrate assay, DH376 and DO34 were also confirmed as potent inhibitors of DAGLβ with IC_{50} values of 1.5-5.6 nM (Figure 1b and Table 1).

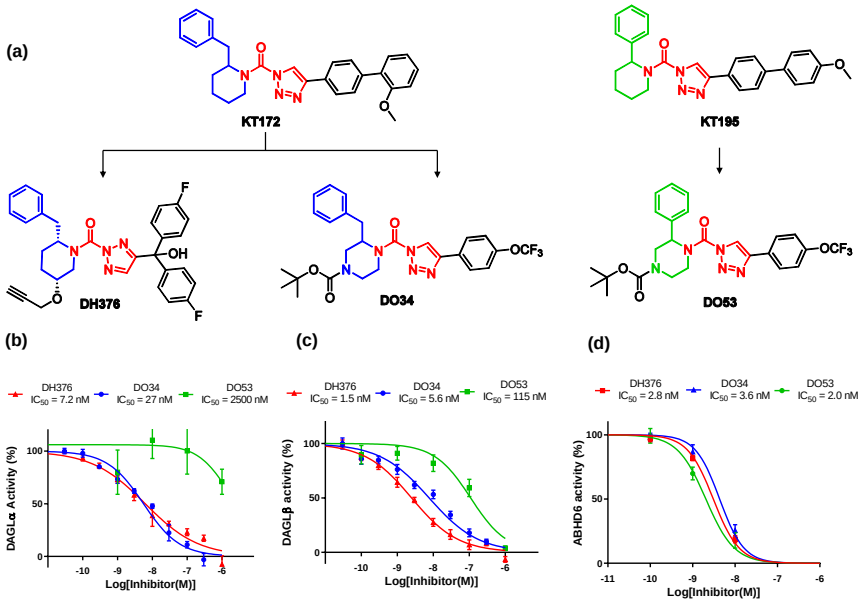

Figure 1. Discovery of triazole urea inhibitors (DH376, DO34) and a control probe DO53 for DAGLs. (a) Chemical structures of original DAGL inhibitor KT172 and structurally related control probe KT195 highlighting conserved features (blue [staying groups, KT172, DH376, DO34], red (triazole urea reactive groups), green (staying groups, KT195 and DO53]) and modifications (black) that furnished potent DAGL inhibitors DH376 and DO34 and the control probe DO53. (b-c) Concentration-dependent inhibition of recombinant human DAGLα (b) and mouse DAGLβ (b) activity by DH376, DO34, and DO53 as measured with a 1-stearoyl-2-arachidonoyl-sn-glycerol (SAG) substrate assay in DAGL-transfected HEK293T cells. Data represent average values ± SD; n = 4 per group. (d) Concentration-dependent inhibition of recombinant human ABHD6 activity by DH376, DO34 and DO53 as measured with 2-AG substrate assay in ABHD6-transfected HEK293T cells. Data represent average values ± SD; n = 4 per group.

Table 1. Inhibitory values for DH376, DO34, and DO53 versus recombinant and native DAGL enzymes using the indicated assays. Data represent average values ± SD; n = 3 per group.

		pIC_{50}	
Enzyme	Compound	DAGLα	DAGLβ
Recombinant enzymes	DH376	8.2 ± 0.3	8.6 ± 0.3
(SAG hydrolysis assay)	DO34	8.2 ± 0.3	8.1 ± 0.3
	DO53	5.6 ± 0.4	7.0 ± 0.2
Brain enzymes			
ABPP (DH379)	DH376	9.2 ± 0.1	8.6 ± 0.1
	DO34	9.1 ± 0.1	8.6 ± 0.1
	DO53	7.4 ± 0.1	7.6 ± 0.1
Brain enzymes			
ABPP (HT-01)	DH376	8.9 ± 0.1	8.3 ± 0.1
	DO34	9.3 ± 0.1	8.6 ± 0.1
	DO53	7.6 ± 0.1	7.1 ± 0.1

DH376 possesses a chiral propargyl ether at the C5 position of the staying group, which may serve as a handle to introduce reporter groups by copper-catalyzed azide-alkyne cycloaddition (CuAAC, or "click") chemistry[31] to generate an additional class of DAGL-tailored activity-based probes for target engagement studies. With this goal in mind a BODIPY-derivatized analog of DH376 was synthesized and termed DH379 (Scheme 1).

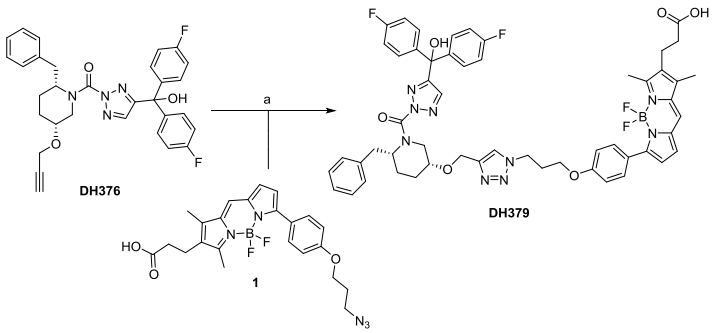

Scheme 1. Synthesis of activity-based probe DH379. Reagents and conditions: (a) $CuSO_4$, sodium ascorbate, DCM/H_2O, r.t., 24h, 32%.

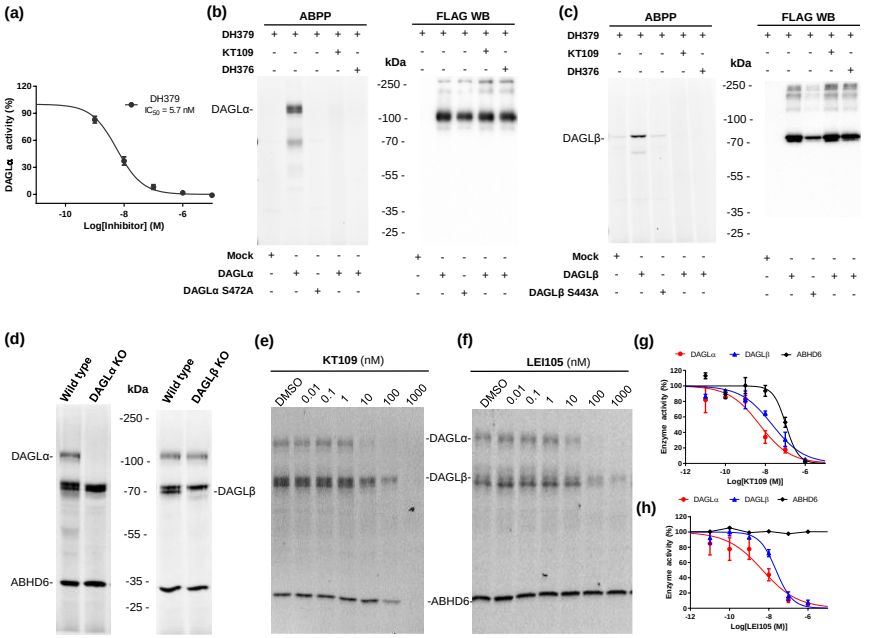

Figure 2. Characterization of DAGLs-tailored activity-based probe DH379. (a) Concentration-dependent inhibition curves against hDAGLα in HEK-293T cell membrane as determined by the PNP colorimetric assay (±SD, n=4). (b-c) Left panels, DH379 labels recombinant, FLAG epitope-tagged wild type DAGLα (b) and DAGLβ (b), but not their catalytically inactive serine mutants (S472A and S443A, respectively) or DAGL enzymes that have been pre-treated with inhibitors KT109 or DH376 (1 µM, 30 min). Right panel, western blots showing DAGL enzyme expression levels in transfected HEK293T cells as determined with an anti-FLAG antibody. (d) Labelling and detection of endogenous DAGLα and DAGLβ in mouse brain membrane proteome by DH379 (1 µM, 20 min). The assignment of DH379-labeled proteins as DAGLα and DAGLβ was confirmed by analyzing brain membrane proteomes from wild type and DAGLα and DAGLβ knockout mice. (e-f) Competitive ABPP with the indicated concentrations of DAGLs inhibitors KT109 (irreversible) (e) and LEI105 (reversible) (f) using ABP DH379 (1 µM, 30 min) in mouse brain membrane proteome. (g-h) Quantification of data shown in (e-f). Data represent average values ± SEM; n = 3 per group.

To validate DH379 as a DAGLα and DAGLβ probe, different hDAGLα and –β constructs were transiently transfected into HEK293T cells (Figure 2). First, it was confirmed that DH379 labeled membrane fractions of hDAGLα-FLAG transfected cells. A strong fluorescence signal was observed at around 120 kDa, which corresponds to the molecular mass of hDAGLα. This band overlapped with a protein visualized by the FLAG-tag antibody and was absent in mock-transfected cells. Pre-incubation of KT109 or DH376 (1 µM, 30 min) inhibited the enzymatic activity and prevented the labeling of the protein at 120 kDa. Site-directed mutagenesis of the catalytic DAGLα nucleophile Ser472 into an alanine abolished labeling of the protein by DH379. Of note, hDAGLα protein expression was not altered by the mutagenesis as determined with the FLAG-tag antibody (Figure 2b). In a similar vein, DH379-mediated labeling of recombinant hDAGLβ was confirmed, (Figure 2c). Mouse

membrane brain proteomes were used to detect labeling of endogenous DAGLα and –β by DH379 (Figure 2d). The fluorescent bands corresponding to DAGLα and – β were absent in proteomes derived from DAGLα, or DAGLβ knockout mice, respectively. In addition to DAGLα and -β, DH379 also labeled two more bands, ~35 kDa (ABHD6) and ~70 kDa (almost overlapped with DAGLβ). Collectively, these data confirm and validate DH379 as a DAGL-tailored activity-based probe.

Competitive activity-based proteome profiling (ABPP) assays were next employed to evaluate the activity and selectivity of DH376 and DO34 against endogenous DAGLs and other serine hydrolases in the mouse brain membrane proteome. These studies were performed with three different activity-based probes: two DAGL-tailored activity based probes – DH379 and HT-01[27] – and a broad-spectrum serine hydrolase-directed probe fluorophosphonate-rhodamine (FP-rhodamine).[32] HT-01 and DH379 provided target engagement assays for DAGLs, while FP-rhodamine assessed cross-reactivity across a broad array of brain serine hydrolases. DH376 and DO34 inhibited DAGLα and β labeling by HT-01 (Figure 3a, b and Table 1) and DH379 (Figure 3C, D and Table 1) with IC_{50} values in the range of 0.4–2.8 (DAGLα) and 0.6-5.8 (DAGLβ) nM, respectively. DO34 and DH376 showed excellent selectivity for DAGLs, with the only detectable serine hydrolase off-targets being ABHD6 and PLA2G7 (Figure 4a). Finally, DH376 and DO34 showed minimal and negligible binding, respectively, to cannabinoid CB_1 (CB_1R) and CB_2 (CB_2R) receptors as measured with radioligand binding assays (IC_{50} values > 1 µM, Figure 4).

Previously, 2-phenyl piperidine analogs, such as KT195[27] (Figure **1a**), were reported to serve as useful inactive control probes that display greatly attenuated inhibition of DAGLs, while maintaining activity against common off-targets like ABHD6.[27] Based on this precedent, DO53 (a 2-phenyl piperazine analog of DO34) was synthesized, and found to exhibit ~100-fold lower activity against DAGLα compared to DO34 or DH376 as measured by DAG substrate hydrolysis (Figure 1b and Table 1) or competitive ABPP assays in mouse brain (Figure 3 and Table 1). On the other hand, DO53 cross-reacted with the shared off-targets of DO34 and DH376 (Figures 1 and 3), designating DO53 as a potentially suitable control compound for biological studies of DAGL enzymes.

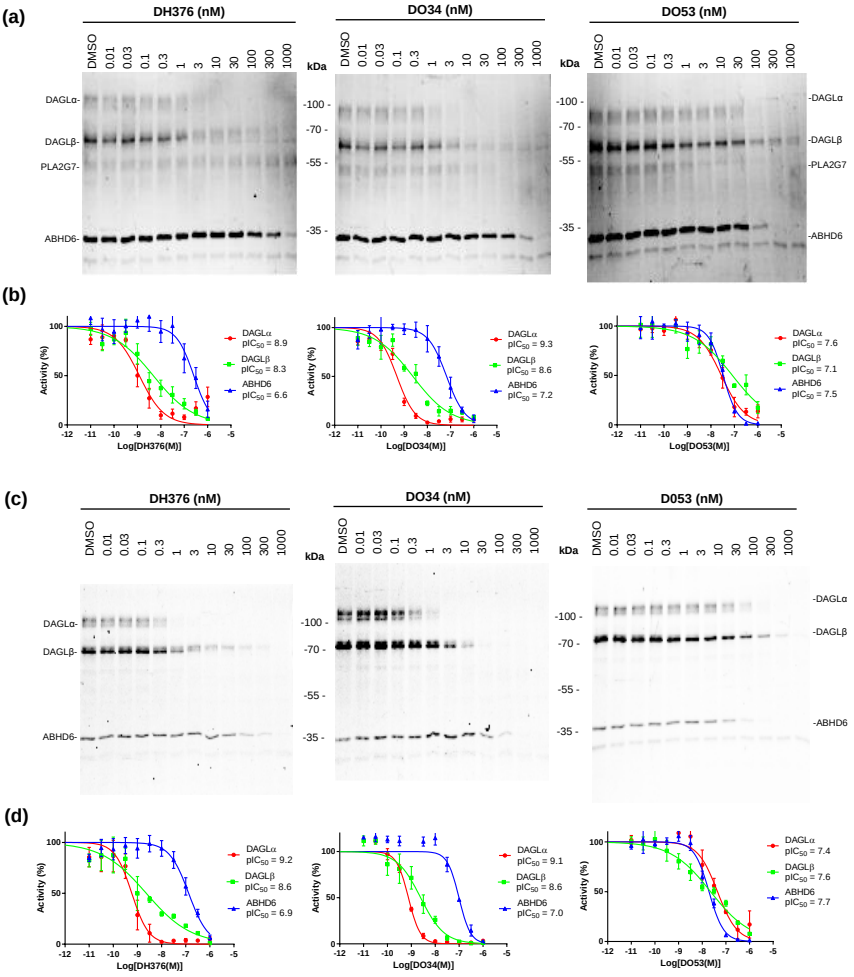

Figure 3. *In vitro* activity characterization of DAGL inhibitors and control probe DO53. (a) Concentration-dependent inhibition of DAGLα and DAGLβ activity by DH376, DO34 and DO53 as measured by gel-based competitive ABPP of mouse brain proteome using the tailored activity-based probe HT-01 (1 μM, 30 min). (b) Quantification of data shown in (a). Data represent average values ± SEM; n = 3 per group. (c) Concentration-dependent inhibition of DAGLα, DAGLβ, and ABHD6 by DH376, DO34 and DO53 as measured by gel-based competitive ABPP of mouse brain proteome using the DH379 probe (1 μM, 30 min). (d) Quantification of data shown in (c). Data represent average values ± SEM; n = 3 per group.

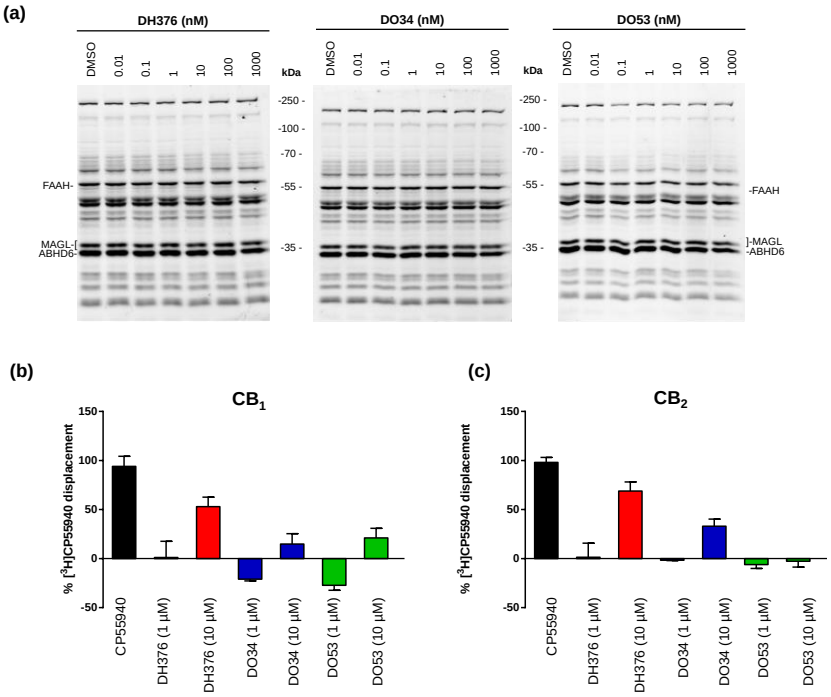

Figure 4. *In vitro* selectivity profiles of DAGL inhibitors and control probe DO53. (a) Selectivity profiles of DH376, DO34, and DO53 across mouse brain serine hydrolases as determined by competitive ABPP using the broad-spectrum probe TAMRA-FP (0.5 µM, 20 min). Representative mouse brain serine hydrolases detected by TAMRA-FP are labeled. Note that, in these gel profiles for TAMRA-FP labeling, the ABHD6 and MAGL signals were not resolved from one another (and DAGLα and DAGLβ are not visualized due to overlapping migration patterns with more abundant serine hydrolases). (b-c) Interactions of DAGL inhibitors and control probe DO53 with cannabinoid receptors (CB_1R and CB_2R). DH376 and DO34 were tested for binding affinity to the CB_1R (b) and CB_2R (c) using competition studies with the radiolabeled CBR ligand [3H]-CP55940 using membranes from recombinant human CB_1R- and CB_2R-overexpressing CHO cells. DO34 was inactive at 10 µM and DH376 was inactive at 1 µM and showed only partial (~50% for CB_1, ~70% for CB_2) inhibition of ligand binding at 10 µM.

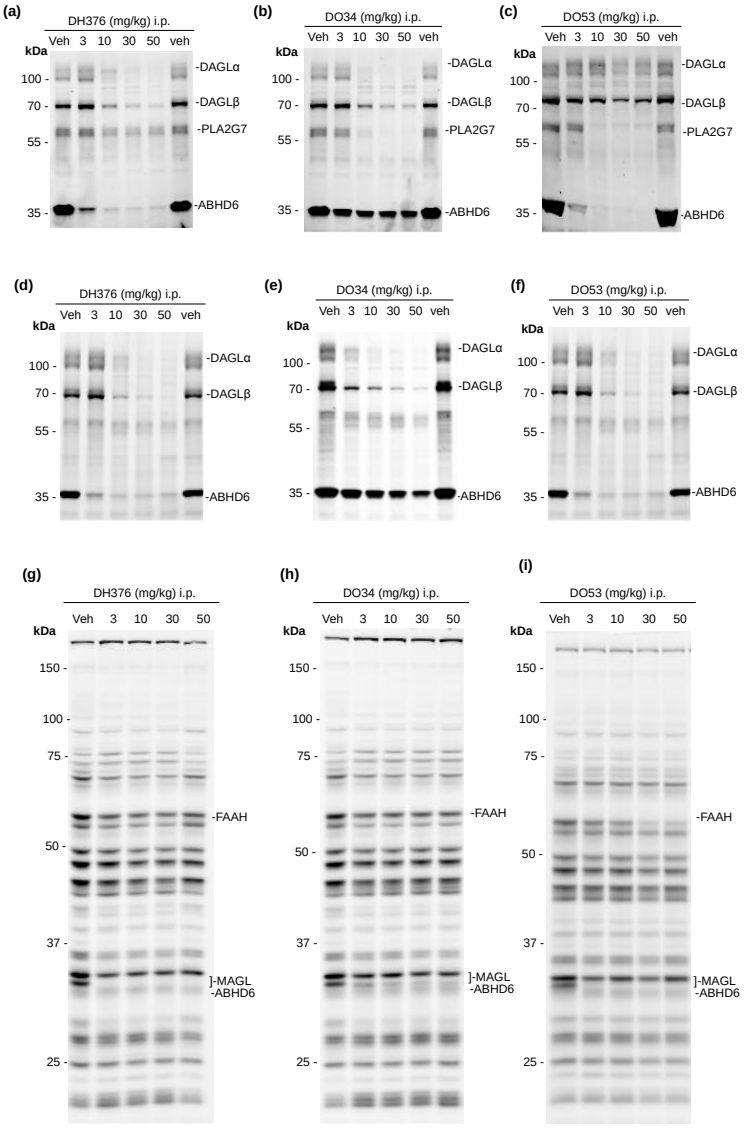

Figure 5. *In vivo* activity and selectivity of DH376, DO34, and DO53 in mice. (a−f) Dose-dependent inhibition of DAGLα and DAGLβ in brain tissue from mice treated with DH376 (a, d), DO34 (b, e), and DO53 (c, f) (indicated doses, i.p., 4 h treatment) as determined by competitive ABPP using DH379 (a-c) and HT-01 (d-f) as probes (1 μM, 30 min). (g-i) Selectivity assessment of cross-reactivity with other serine hydrolases in brain tissue from mice treated with vehicle (Veh) or DH376 (g), DO34 (h), or DO53 (i) (i.p., 4 h) as determined by competitive ABPP using the TAMRA-FP probe (1 μM, 30 min).

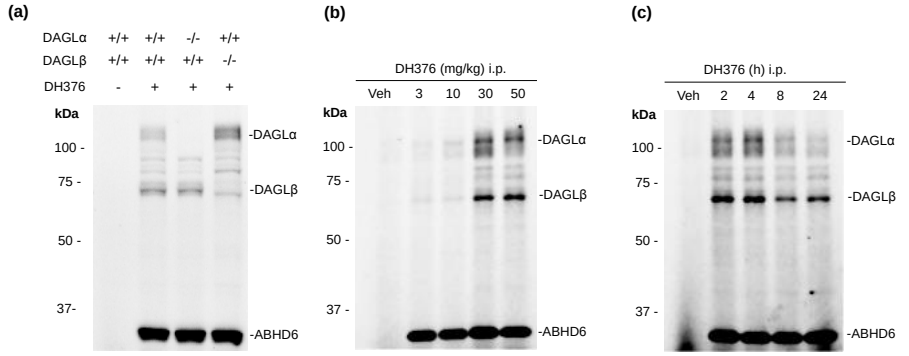

Figure 6. *Ex vivo* Click Chemistry ABPP (CuAAC) analysis of DH376-treated mice. (a) Confirmation of direct, *in vivo*-labeling of DAGLα and DAGLβ by DH376 (50 mg/kg, i.p., 4 h) visualized by CuAAC to a Cy5 reporter group. The assignment of DH376-labeled proteins as DAGLα and DAGLβ was confirmed by analyzing brain membrane proteomes from wild type and DAGLα$^{-/-}$ and DAGLβ$^{-/-}$ mice. (b, c) Dose dependency (b) and time course (c) of direct, *in vivo*-labeling of DAGLα and DAGLβ ABPP in brain tissue from mice treated with DH376 (i.p., 4 h for dose-dependency; 50 mg/kg, i.p. for time-course) visualized by CuAAC to a Cy5 reporter group.

DAGL inhibitors are centrally active *in vivo*

DH376, DO34, DO53 or vehicle was administered intraperitoneally (i.p.) to male C57Bl/6 mice across a dose range of 3 to 50 mg/kg. After 4h, the animals were sacrificed and brain tissue analyzed by competitive ABPP with DH379, HT-01, and TAMRA-FP, which revealed clear dose-dependent blockade of DAGLα activity for both DH376 and DO34 with ED_{50} values of 5-10 mg/kg (Figure 5) and full inhibition of the enzyme being observed at 30-50 mg/kg of inhibitor. DAGLβ (and ABHD6) were also inhibited by DH376, and to a lesser extent by DO34, which instead exhibited cross-reactivity with PLA2G7 (Figure 4a). DO53, on the other hand, did not substantially inhibit DAGLα or DAGLβ at any dose tested, but inhibited both ABHD6 and PLA2G7 (Figure 5). Brain proteomes from DH376-treated mice were conjugated to a Cy5 fluorophore by CuAAC, which confirmed direct, dose-dependent labeling of DAGL enzymes (Figure 6).

These target engagement profiles were confirmed and extended by performing ABPP coupled to high-resolution, quantitative mass spectrometry (MS). In brief, brain proteomes from inhibitor- and vehicle-treated mice were incubated with the serine hydrolase-directed activity-based probe fluorophosphonate (FP)-biotin,[33] and probe-labeled enzymes were enriched by streptavidin chromatography, digested on bead with trypsin, and the resulting tryptic peptides modified by reductive dimethylation (ReDiMe) of lysine residues using isotopically heavy and light formaldehyde, respectively.[34] In these experiments, inhibited serine hydrolases are

identified as enzymes showing low heavy/light ReDiMe ratios. Quantitative MS confirmed complete inhibition of DAGLα by DH376 and DO34, with DAGLβ also being strongly and partially inhibited by these compounds, respectively, and revealed the following off-targets (defined as serine hydrolases with heavy/light ratios < 0.5): ABHD6 (DH376, DO34), CES1C (DH376, DO34), ABHD2 (DO34), BCHE (DH376), LIPE (DH376), PAFAH2 (DO34), and PLA2G7 (DO34) (Figure 7a and 7b). DO53 showed negligible activity against DAGLα or DAGLβ (heavy/light ratios of ~0.8), but cross-reacted with many of the off-targets of DH376 and DO34 (ABHD2, ABHD6, CES1C, PLA2G7, PAFAH2) (Figure 7c and 7d). Taken together (Figure 7d), these competitive ABPP studies designated DH376 and DO34 as *in vivo*-active inhibitor with complementary selectivity profiles that, when used in combination with the control probe DO53, can report on the function of DAGLs in the CNS.

Next, the time course of DAGL inhibition in mice was investigated. At a high dose (50 mg/kg), DH376 and DO34, but not DO53, demonstrated sustained inhibition of DAGLs for up to 8 h, with partial recovery at 24 h post-dosing (Figure 8a-c). Interestingly, a lower dose of DH376 (3 mg/kg) produced substantial inhibition of DAGLα within 30 min after administration, but enzyme activity quickly recovered by 4h (Figure 8g and h). In contrast, DAGLβ was only partly inhibited at 3 mg/kg (Figure 8g), while the off-target ABHD6 remained inhibited up to 8h (Figure 8g and h). These differences in the duration of target engagement were confirmed by *ex vivo* CuAAC-mediated conjugation of a Cy5-azide tag to brain proteomes of DH376-treated mice, which showed strong, but transient DH376 labeling of DAGLα and sustained reactivity with ABHD6 (Figure 8i and j). The recovery of DAGLα activity in this time course study at low drug dose could indicate that DAGLα is a short half-life protein that is rapidly degraded and replaced by newly synthesized enzyme or that the DH376-DAGLα interaction is reversible. Arguing against the latter hypothesis, however, was the observations that the inhibition and direct labeling of DAGLα by DH376 were maintained after size exclusion chromatography, which contrasted with the substantial rescue of DAGLα activity observed in this experiment with the reversible inhibitor LEI-105[35] (Figure 9). DH376, but not LEI-105 also showed a time-dependent increase in potency against DAGLα (Figure 9), another hallmark of an irreversible mechanism of action. The results thus support that DAGLα is a short half-life protein in the CNS and further demonstrate that sustained inhibition of DAGLα for many hours can be achieved at higher doses of DH376 and DO34 (50 mg/kg), where presumably sufficient drug remains in the CNS to block newly synthesized DAGLα protein.

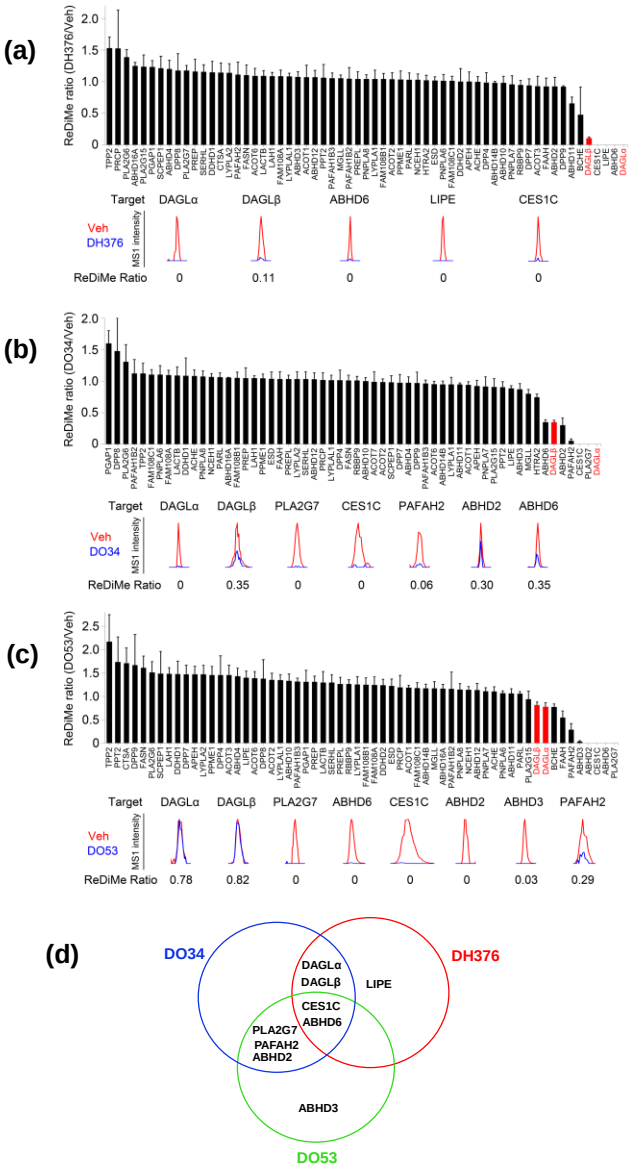

Figure 7. Assessment of *in vivo* activity and selectivity of DH376, DO34 and DO53 by ABPP-ReDiMe analysis. ABPP-ReDiMe analysis of brain serine hydrolase activities from mice treated with DH376 (a), DO34 (b) and DO53 (c) (50 mg/kg, i.p., 4 h treatment), where serine hydrolases were labeled and enriched using an FP-biotin probe. Representative MS1 chromatograms for DAGLα and DAGLβ, as well as additional serine hydrolase targets are shown for each inhibitor. Data represent average values ± SEM; n = 4 mice per group. (d) Summary of the serine hydrolase targets of DH376, DO34, and DO53 in mouse brain. Serine hydrolases with ReDiMe ratio values < 0.5 were defined as targets for each inhibitor. Note that the DAGLα and DAGLβ are the only two serine hydrolases found to be inhibited by both DH376 and DO34, but not DO53, in mouse brain.

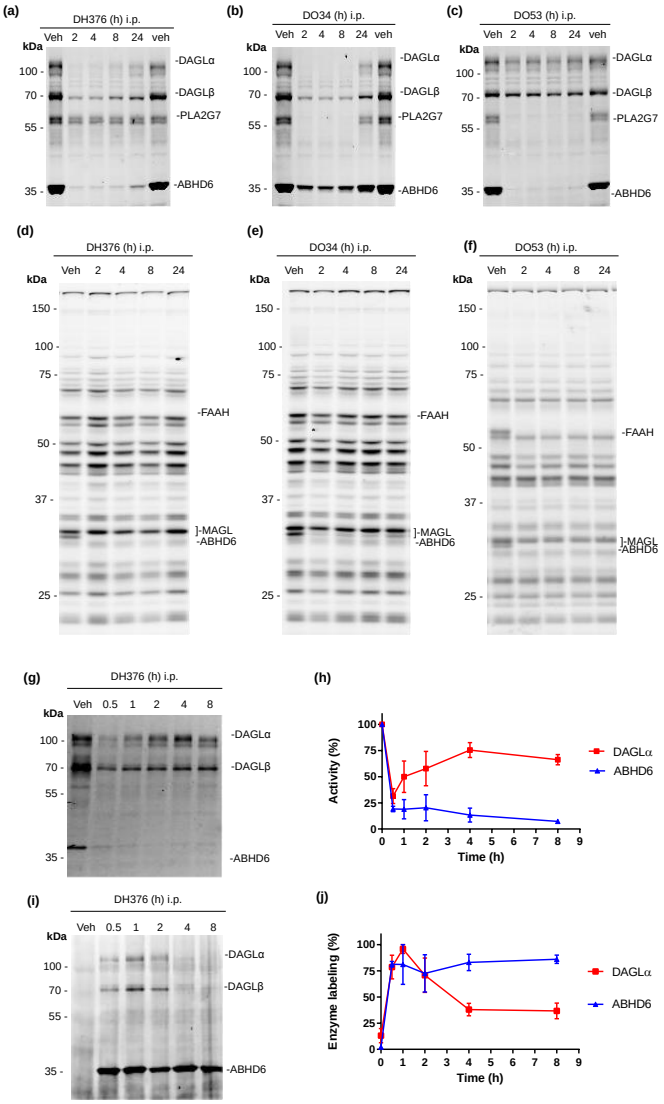

Figure 8. *In vivo* time course analysis of DAGLα inhibition and recovery. (a-f) Assessment of time-course of inhibition of DAGLα and DAGLβ (a-c) and cross-reactivity with other serine hydrolases (d-f) in brain tissue from mice treated with vehicle or DH376 (a, d), DO34 (b, e) or DO53 (c, f) (50 mg/kg, i.p.) as determined by competitive ABPP using the HT-01 (a-c) or TAMRA-FP (d-f) probe (1 μM, 30 min). (g, h) Time course of inhibition of DAGLα in brain tissue from mice treated with a low dose of DH376 (3 mg/kg, i.p.) as determined by competitive ABPP using the DH379 probe (1 μM, 30 min). Gel data (g) and quantification of these data (h) relative to a vehicle-treated control group are shown for both DAGLα and ABHD6, an off-target of DH376. Data represent average values ± SEM; n = 3 mice per group. (i, j) Time course of direct labeling of DAGLα in brain tissue from mice treated with DH376 (3 mg/kg, i.p.) visualized by CuAAC to a Cy5 reporter group. Gel data (i) and quantification of these data (j) relative to a vehicle-treated control group are shown for both DAGLα and ABHD6. Data represent average values ± SEM; n = 3 mice per group.

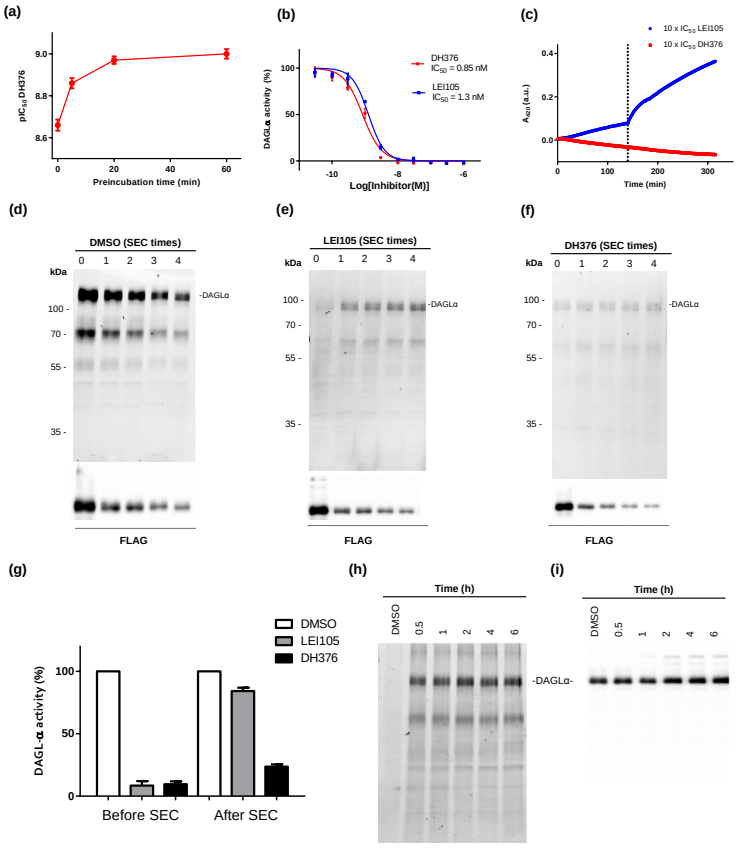

Figure 9. (a) Plot of IC_{50} values for DH376 inhibition of DAGLα measured after the indicated pre-incubation times prior to analysis with a para-nitrophenylbutyrate (PNP) substrate (300 μM). Data represent average values ± SEM; n = 4 per group. (b) Concentration-dependent inhibition of recombinant human DAGLα activity by DH376 and LEI105 (reversible DAGLα inhibitor). Data represent average values ± SEM; n=4 per group. (c) DAGLα product progression curves as a function of time in the presence of PNP substrate (300 μM) and 10 x IC_{50} value concentrations of LEI105 or DH376. After 135 min, a second batch of PNP (300 μM) was added to the reaction vessel. Note that the enzymatic rate of PNP conversion is increased in the LEI105-treated sample (blue line), whereas no effect is observed in enzyme inhibited by DH376 (red line). Shown is a representative experiment of four replicate experiments. (d-f) Recovery of DAGLα activity after exposing the indicated inhibitor (or control)-treated samples to serial size exclusion chromatography (SEC) steps, where activity was measured by gel-based ABPP using probe DH379. Note that little or no DH379 labeling was observed post-SEC in DH376-treated DAGLα samples (f), while substantial MB064 labeling was observed post-SEC for DAGLα samples treated with the reversible inhibitor LEI105 (e). Western blots using anti-FLAG antibodies are shown to assess protein loading. (g) Quantification of the data shown in (d-f) after four SEC steps. Data represent average values±SD; n=3 per group. (h) Assessment of stability of the DH376-DAGLα adduct. Recombinant human DAGLα expressed in transfected HEK293T cell proteomes was treated with DH376 (10 nM) for 30 min and the reaction was exposed to five serial SEC steps and then incubated for the indicated times (0.5-6h) before visualization by CuAAC to a Cy5 reporter group. No appreciable loss of signal intensity for the DH376-DAGLα adduct was observed across the time course analysis. (i) Western blot using anti-FLAG antibodies is shown to assess protein loading.

DAGL inhibitors rapidly and radically alter brain lipid profiles in mice

Three independently generated lines of DAGLα$^{-/-}$ mice have shown that genetic disruption of this enzyme substantially reduces brain 2-AG (~80-90%).[13,14,17,36] These brain 2-AG changes are accompanied by concomitant accumulation of the main 2-AG lipid precursor and protein kinase C (PKC) agonist[37] 1-stearoyl-2-arachidonoylglycerol (SAG)[17] and depletion of the principal 2-AG hydrolytic metabolite and eicosanoid precursor, arachidonic acid (AA)[13,14,17] as well as of the second major endocannabinoid anandamide (AEA)[13,14]. It remains unclear, however, what portion of these widespread alterations reflects the active and dynamic regulation of brain lipid signaling networks by DAGLα versus adaptive changes caused by the constitutive, long-term ablation of this enzyme. This question was therefore addressed by examining the brain lipid profiles of mice treated with the CNS-active DAGL inhibitors DH376 and DO34 and the control probe DO53.

First, the brain lipid profiles of mice were analyzed by LC-MS at a single 4h time point post-dosing with inhibitors (50 mg/kg, i.p.). This revealed dramatic reductions in 2-AG in DH376- and DO34- but not DO53-treated mice (Figure 10a). This reduction in 2-AG was comparable in magnitude to that observed in DAGLα$^{-/-}$ mice (Figure 10a), demonstrating the rapid flux of DAGL-mediated 2-AG production *in vivo*. The robust depletion of brain 2-AG in DH376- and DO34-treated mice was dose-dependent (Figure 10h and i) and was observed within 2 h after injection. The time-dependent changes in 2-AG caused by DH376 appeared to be shorter-lived than those of DO34 (Figure 10g and j). Notably, DH376 and DO34 also caused rapid, dose-dependent changes in other DAGL-regulated lipids, including reductions in AEA (Figure 10b and h-j), AA (Figure 10c and h-j), and the prostaglandins PGD_2 and PGE_2 (Figure 10d, e and h-j), as well as elevations in SAG (Figure 10f and h-j) and C18:1/C20:4 DAG (Figure S1.; Table 2). The changes in each lipid species were again similar in magnitude to those observed in DAGLα$^{-/-}$ mice (Figure 8b-f), were dose-dependent (Figure 8h and f), displayed similar time courses to alterations observed in 2-AG in DH376- and DO34-treated mice (Figure 8g and j), and were absent in DO53-treated mice (Figure 8a-f). While most lipid changes were consistent between DAGL inhibitor-treated and DAGLα$^{-/-}$ mice, it was found that DAGLα$^{-/-}$ mice showed reductions in triglycerides (TAGs), that were not observed in animals treated with DAGL inhibitors (Figure S2). These alterations in TAGs may thus require chronic, long-term inactivation of DAGLα, which is also known to cause significant reductions in total body weight and fat.[15]

These studies, taken together, demonstrate that acute pharmacological blockade of DAGLs produces a rapid and dramatic reorganization of lipid signaling networks in the mammalian brain that largely mirrors the myriad lipid changes observed in the brains of DAGLα$^{-/-}$ mice. Accordingly, it was then asked whether DH376 and DO34 would affect physiological processes that involve one or more components of the DAGL-regulated lipid signaling network.

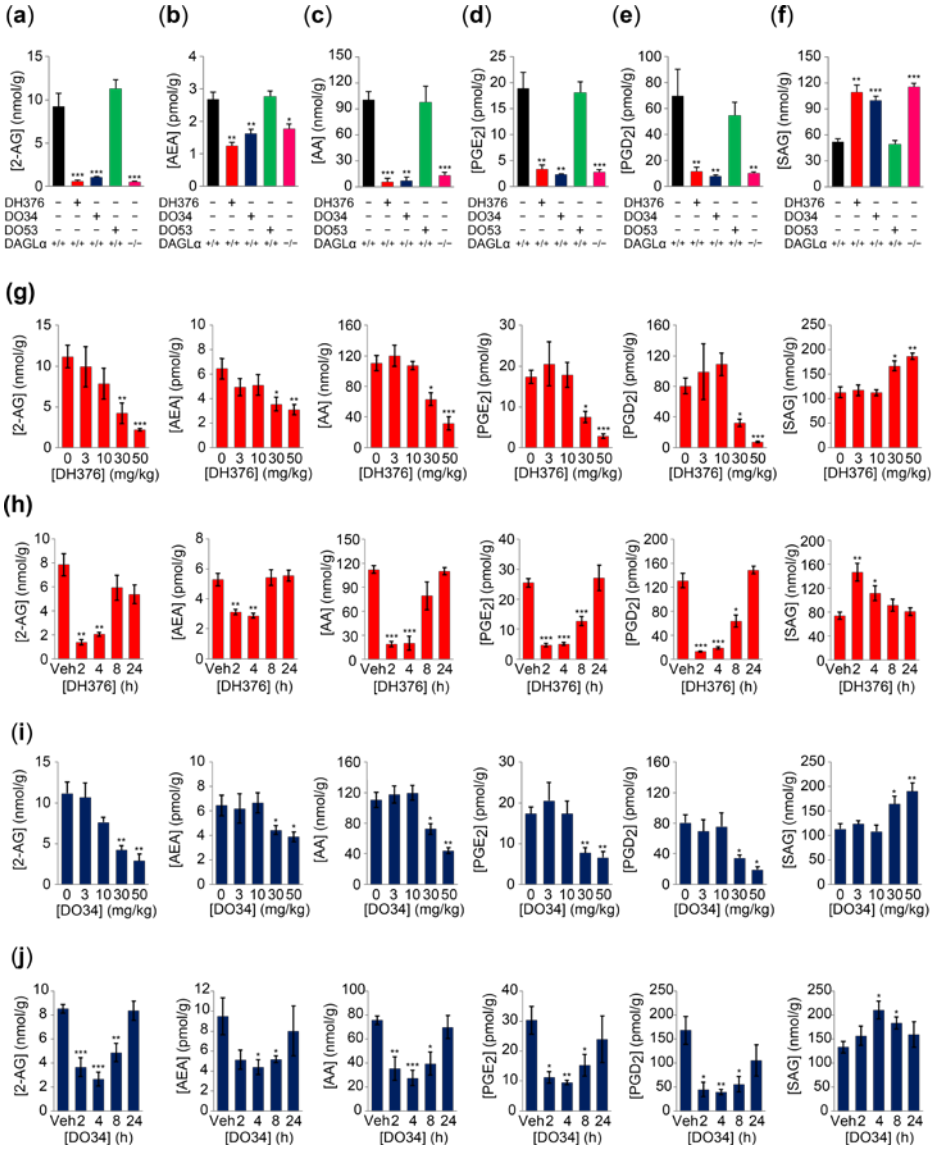

Figure 10. Acute inhibition of DAGLs causes rapid and profound remodeling of bioactive lipid pathways in the brain. (a-f) Quantification of 2-AG (a) and related bioactive lipids (b-f) in brain tissue from mice treated with vehicle or DH376, DO34, and DO53 (50 mg/kg, i.p., 4 h). Lipid profiles from DAGLα$^{-/-}$ mice are shown for comparison. Data represent average values ± SEM; n = 5–6 mice per group. *P < 0.05; **P < 0.01; ***P < 0.001 for inhibitor treated DAGLα$^{+/+}$ mice or DAGLα$^{-/-}$ mice vs. vehicle treated DAGLα$^{+/+}$ mice. (g, i) Dose-dependent changes in 2-AG and other bioactive lipids in brain tissue from mice treated with DH376 (g) and DO34 (i) (i.p., 4 h). Data represent average values ± SEM; n = 4−5 mice per group. *p < 0.05; **p < 0.01; ***p < 0.001 for inhibitor-treated vs vehicle-treated (0 mg/kg) mice. (h, j) Time-dependent changes in 2-AG and other bioactive lipids in brain tissue

from mice treated with DH376 (h) and DO34 (j) (50 mg/kg, i.p.). Data represent average values ± SEM; n = 4−5 mice per group. *p < 0.05; **p < 0.01; ***p < 0.001 for inhibitor treated vs. vehicle-treated mice.

DAGL inhibitors block endocannabinoid-dependent synaptic plasticity

2-AG functions as a major retrograde messenger at synapses throughout the brain that acts on presynaptically localized CB_1Rs to suppress neurotransmitter release.[20] Various forms of synaptic plasticity are regulated by 2-AG signaling, including depolarization-induced suppression of excitation (DSE) and inhibition (DSI),[20] both of which are abolished in DAGLα$^{-/-}$ mice.[13,14] Interestingly, however, conflicting findings have emerged about whether the retrograde signaling 2-AG is biosynthesized by DAGLα on-demand or alternatively pre-synthesized and stored within neurons prior to stimulus-induced release.[21-23,25] As noted by others,[21] these differences may reflect the poor physicochemical properties of the DAGL inhibitors used in past studies, as the high lipophilicity of these molecules could limit their penetration into brain tissue preparations used to measure DSI and DSE, resulting in incomplete inhibition of DAGLs. Therefore, the effects of DH376, DO34 and DO53 in models of endocannabinoid-dependent synaptic plasticity were tested.

DSE at parallel fiber (PF) to Purkinje cell (PC) synapses in acute cerebellar slices were first examined. A brief depolarization of PCs induced robust transient DSE at PF-PC synapses in vehicle-treated cerebellar slices (Figure 9a and b). Bath application of DH376 (1-10 µM) or DO34 (0.1-1 µM) to cerebellar slices 30 min prior to starting electrophysiological recordings blocked DSE in a concentration-dependent manner with a half-maximal inhibition of 1.1 µM and 0.18 µM, respectively (Figure 11a and b). The control probe DO53 did not alter cerebellar DSE (10 µM, Figure 11a and b). Then, DSI at CA1 pyramidal neuron synapses in hippocampal slices were evaluated. DSI was induced in vehicle-treated hippocampal slices by applying a brief depolarization while evoking IPSCs through stimulation of synaptic inhibitory inputs (Figure 11c and d). Bath application of DH376 (10 µM) and DO34 (1 µM), but not DO53 (10 µM), for 30 min prior to starting electrophysiological recordings fully blocked hippocampal DSI (Figure 11c and d).

These results support a model where the 2-AG that regulates both DSE and DSI forms of synaptic plasticity in the brain is produced on-demand by DAGLα.

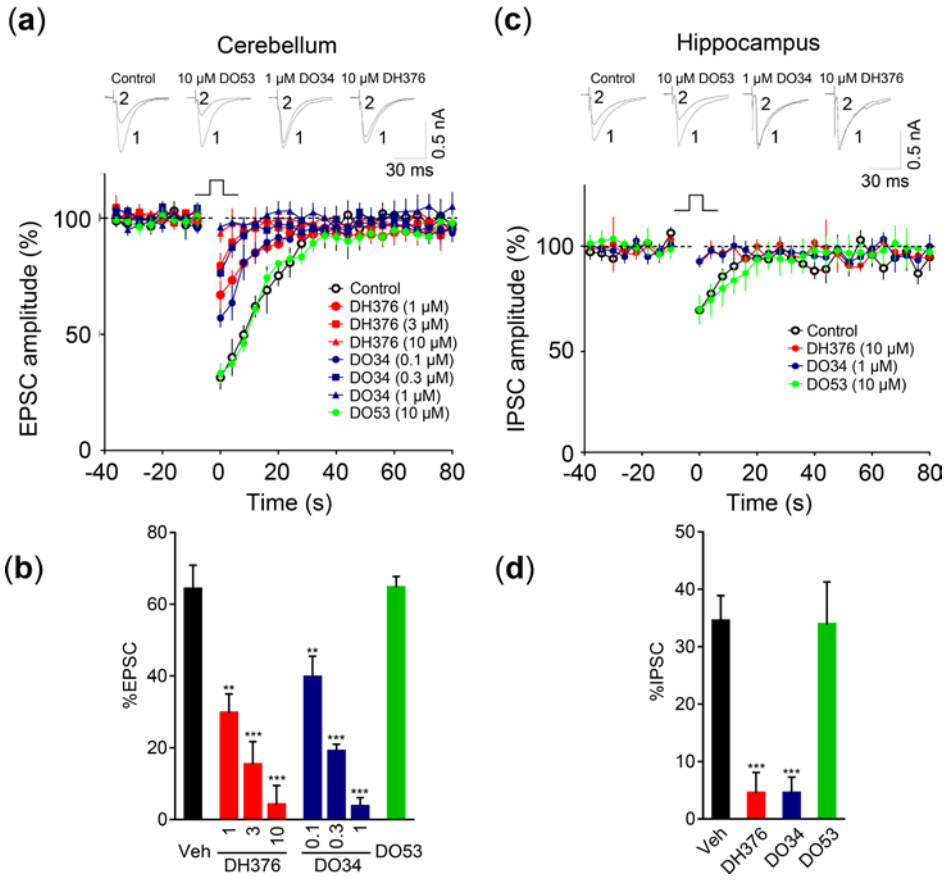

Figure 11. Acute inhibition of DAGLs fully blocks endocannabinoid-mediated forms of synaptic plasticity. (a, b) Sample traces and average time course (a) and magnitude (b) of parallel fiber-excitatory postsynaptic currents (PF-EPSCs) in response to a brief depolarization in cerebellar slices following treatment (30 min) with vehicle, DH376 (1-10 μM), DO34 (0.1−1 μM), or DO53 (10 μM). Data represent average values ± SEM; n = 5-10 samples per group. (c, d) Sample traces and average time course (c) and magnitude (d) of inhibitory postsynaptic currents (IPSCs) in CA1 pyramidal neurons in response to a brief depolarization in hippocampal slices following treatment (30 min) with vehicle, DH376 (10 μM), DO34 (1 μM), and DO53 (10 μM). Data represent average values ± SEM; n = 7−8 samples per group. *p < 0.05; **p < 0.01; ***p < 0.001 vs. vehicle-treated samples.

DAGL inhibitors attenuate neuroinflammatory responses *in vivo*

MAGL-mediated hydrolysis of 2-AG provides a major source of AA substrate for prostaglandin synthesis in the nervous system under basal and neuroinflammatory states.[38-41] Having discovered that acute, pharmacological inhibition of DAGLs coordinately lowers 2-AG and prostaglandin content of the brain (Figure 8), next it was asked whether blocking these enzymes affects neuroinflammatory processes

regulated by these bioactive lipids. High-dose lipopolysaccharide (LPS) treatment induces brain prostaglandin and cytokine production[38,41] and leads to profound anapyrexia in rodents,[42,43] an effect that is thought to be mediated, at least in part, by centrally produced prostaglandins and endocannabinoids.[42] MAGL blockade has been shown to suppress LPS-induced prostaglandin and cytokine production in the CNS,[38,41] but also exacerbates the anapyrexia observed in this paradigm through a CB_1R-dependent mechanism.[43] Building on these observations, the effects of pharmacological and genetic inactivation of DAGL activity were examined on neuroinflammatory responses induced by LPS.

Mice were treated with DH376, DO34, DO53 (50 mg/kg, i.p) or vehicle (60-90 min), followed by LPS (20 mg/kg, i.p., 6 h) or vehicle, and then sacrificed and their brain lipid and cytokine profiles analyzed. As expected, DH376- and DO34-treated mice, as well as DAGLα$^{-/-}$ mice, but not DO53-treated mice, exhibited severely depleted brain 2-AG (Figure 12a), AA (Figure 12c), and PGE_2 (Figure 12d) under basal control conditions. LPS treatment caused a modest, but significant increase in 2-AG (Figure 12a), a reduction in AA (Figure 12c), and a substantial increase in PGE_2 (Figure 12e). The LPS-induced elevations in both 2-AG and PGE_2 were strongly suppressed in DH376- and DO34-treated mice and DAGLα$^{-/-}$ mice, but not DO53-treated mice. LPS treatment also increased brain cytokines, and this effect was significantly attenuated in DAGLα$^{-/-}$ mice (Figure 12f-h). DH376- and DO34-treated mice also showed reductions in LPS-stimulated brain cytokines, but interpreting these effects proved complicated because the control probe DO53 also blocked brain cytokine production to a similar degree (Figure 12f-h). These data could indicate that one or more of the off-targets shared by the DAGL inhibitors and DO53 also participates, along with DAGLα (as supported by studies in DAGLα$^{-/-}$ mice), in LPS-induced cytokine production, or that active metabolites of the inhibitors may suppress cytokines. Finally, it was found that LPS-induced anapyrexia was substantially blunted in DH376- and DO34-treated mice (Figure 13a) and DAGLα$^{-/-}$ mice (Figure 13b), but not DO53-treated mice (Figure 13a).

These results, when combined with previous findings,[38,41,43] indicate that blockade of the principal 2-AG biosynthetic and degradation enzymes in the brain, DAGLα and MAGL, respectively, produces overlapping (reductions in brain prostaglandins and cytokines), but distinct (suppression versus enhancement of anapyrexia) effects on LPS-induced neuroinflammation.

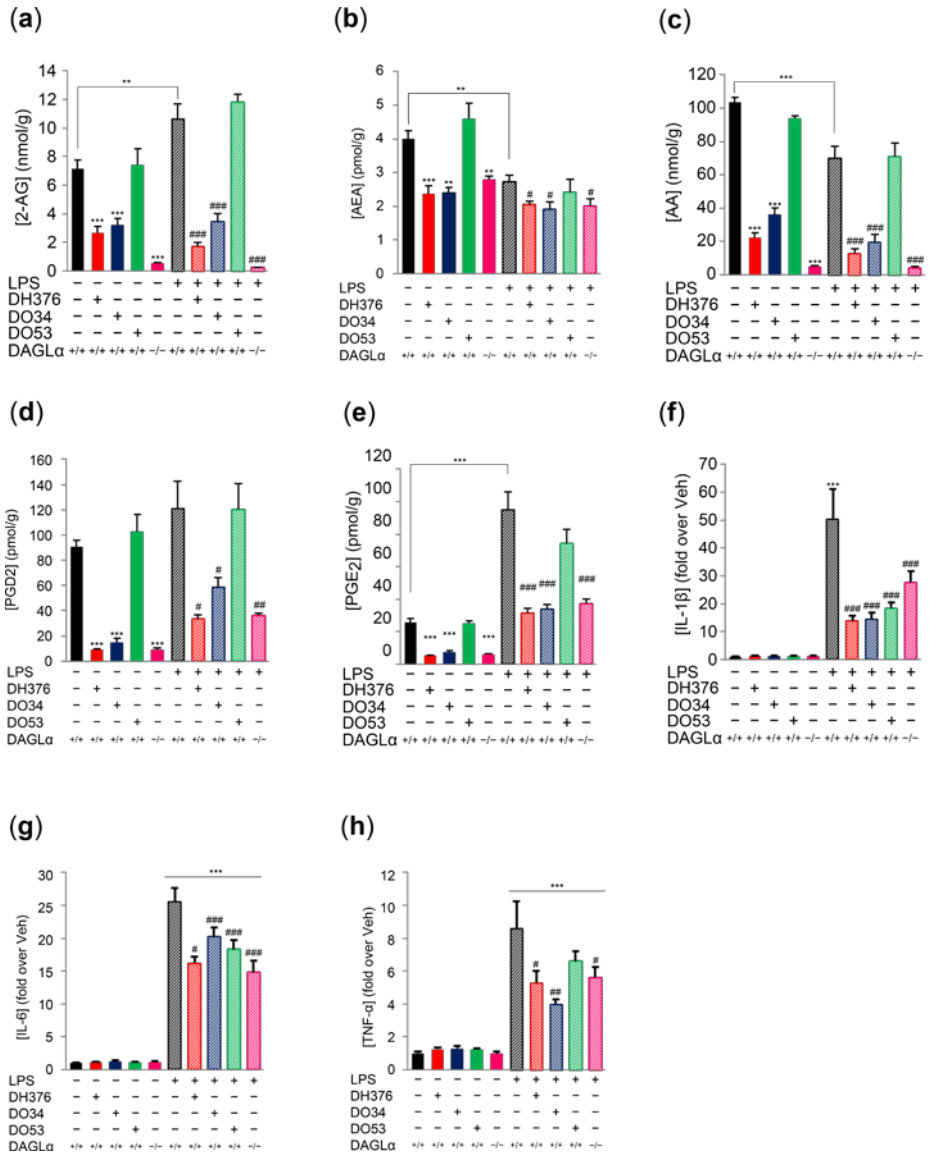

Figure 12. Disruption of DAGLs reduces brain inflammatory cytokine production in LPS-treated mice. (a−e) Quantification of 2-AG and related bioactive lipids in brain tissue from vehicle- or DH376-, DO34-, and DO53-treated (50mg/kg, i.p., 1−1.5 h) or DAGLα$^{-/-}$ mice with or without subsequent treatment with LPS (20 mg/kg, i.p., 6 h). (f-h) Quantification of the IL-1β (f), IL-6 (g) and TNF-α (h) cytokines from DH376-, DO34-, and DO53-treated (50 mg/kg, i.p., 1−1.5 h) or DAGLα$^{-/-}$ mice with or without subsequent treatment with LPS (20 mg/kg, i.p., 6 h). Data represent average values ± SEM; n = 5−8 mice per group. **P < 0.01; ***P <0.001 for all groups vs. vehicle-treated DAGLα$^{+/+}$ mice and $^{###}$P < 0.001 for all groups compared with LPS-treated DAGLα+/+ mice.

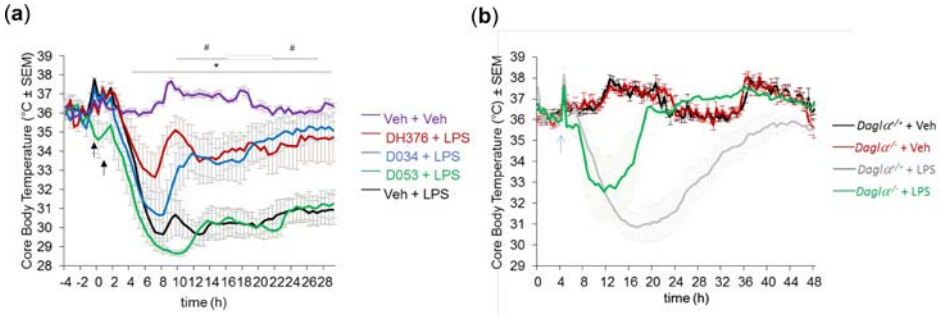

Figure 13. Acute inhibition of DAGLs suppresses LPS-induced neuroinflammatory responses in mouse brain. (a, b) Time course of body temperature changes for mice pretreated with vehicle or DH376, DO34, and DO53 (a) or for DAGLα$^{+/+}$ and DAGLα$^{-/-}$ mice (b) following LPS treatment (10 mg/kg, i.p.). Data represent average values ± SEM; n = 5−6. For E, *P < 0.05 Veh + Veh vs. Veh + LPS group; #P < 0.05 for DH376 + LPS and DO34 + LPS vs. Veh + LPS group. For F, *P < 0.05 for DAGLα$^{+/+}$ + Veh vs. DAGLα$^{+/+}$ + LPS groups; $^{\#}$P < 0.05 for DAGLα$^{-/-}$ + Veh vs. DAGLα$^{-/-}$ + LPS groups; $^{\&}$P < 0.05 for DAGLα$^{-/-}$ + LPS vs. DAGLα$^{+/+}$ + LPS groups.

Discussion

Endocannabinoids regulate synaptic activity throughout the CNS and impact diverse physiological and behavioral processes.[44,45] Inhibitors of enzymes that degrade endocannabinoids have proven useful for elucidating the neurobiological and behavioral effects caused by heightened endocannabinoid activity.[46] It has been more challenging, however, to determine the biological impact of reducing endocannabinoid function due in large part to a lack of selective and CNS-active inhibitors that can block endocannabinoid production *in vivo*. While DAGLα$^{-/-}$ and DAGLβ$^{-/-}$ mice have provided valuable models for investigating the *in vivo* effects of disrupting endocannabinoid biosynthesis, DAGLα plays an important role in brain development[13] and chronic alterations in endocannabinoid tone can lead to substantial CB_1R adaptations in the CNS[47,48] and peripheral tissues.[49] The endocannabinoid system also crosstalks with several other bioactive lipid pathways.[8,50,51] The extent to which this larger lipid network is dynamically regulated in the CNS by acute disruption of endocannabinoid synthesis remains unknown. Here these important questions have been addressed by developing CNS-active irreversible DAGL inhibitors - DH376 and DO34 – along with a structurally related control probe DO53. Key to the development of these chemical probes was the use of both broad-spectrum and tailored ABPP probes for assessing selectivity and DAGL inhibition *in vivo*.

Administration of DH376 and DO34 to mice revealed that brain 2-AG content is rapidly and dramatically reduced following acute inactivation of DAGLα. Both inhibitors also produced near-complete blockade of cerebellar DSE and hippocampal DSI, two forms of CB_1R-mediated synaptic plasticity,[20] following only a 30 minute incubation in

brain slices. These results provide strong experimental support for an on-demand model of endocannabinoid biosynthesis[21] versus alternative hypotheses invoking 2-AG storage and release. DAGL inhibitors and tailored activity probes were also used to discover that DAGLα is a short half-life (< 4 h) protein in the CNS. The factors that regulate DAGLα turnover in brain cells remain unknown, but previous studies have shown that DAGLα localization and activity are regulated by interacts with scaffolding proteins[52] and phosphorylation by CamKII.[53] It is possible that such protein-protein interactions and post-translational modifications (> 30 phosphorylation sites have been identified in DAGLα) regulate DAGLα half-life in brain cells. Endocannabinoid-mediated synaptic plasticity has also been shown to depend on transcription and translation in the post-synaptic neuron,[54] which is consistent with the observation of rapid, ongoing production of new DAGLα protein (Figure 9) that generates a strong, tonic flux of 2-AG in the brain (Figure 10). Modulating the half-life of DAGLα may thus provide neurons with a mechanism to influence the magnitude and duration of 2-AG signaling and associated physiological processes, such as learning and memory, which have been shown to require protein synthesis and degradation.[55]

That the profound reduction in 2-AG caused by DAGL inhibitors was accompanied by alterations in DAGs, arachidonic acid, prostaglandins, and other endocannabinoids (AEA) underscores the remarkable integration of lipid signaling networks in the brain and the key role that DAGLs play in orchestrating this crosstalk. Although it can be interpreted that many of the lipid changes caused by DAGL inhibitors reflect the direct flux of substrate and products through interconnected metabolic pathways,[19] others (e.g., AEA reductions) may be the indirect consequence of alterations in lipid signaling. Such signaling-related crosstalk between endocannabinoids has also been reported for AEA action on TRPV1 channels, which can influence 2-AG production in the brain.[56] Regardless of the precise mechanisms by which DAGLs exert their profound influence over brain lipid networks, the data present in this chapter emphasize that the interpretation of phenotypes caused by DAGL disruption should take into consideration more than just impairments in endocannabinoid signaling. In this regard, the data here, combined with previous studies,[43,57] suggest that the attenuated neuroinflammatory responses in DAGLα-disrupted mice likely reflect the integrated outcome of lowering both endocannabinoids and eicosanoids in the brain, although the additional impact of altering DAG-mediated PKC signaling and/or other lipid processes cannot be excluded. Additionally, the discovery here that the control probe DO53 attenuates LPS-induced cytokine production without altering brain prostaglandins or anapyrexia indicates that the various neuroinflammatory effects of LPS can be mechanistically uncoupled.

Taken together, the studies in this chapter demonstrate that DH376 and DO34, along with the control probe DO53 and tailored DAGL activity probes, such as DH379, constitute a valuable chemical tool kit for studying diverse aspects of DAGL function and regulation both in animals and *ex vivo* brain preparations. Projecting forward, this

toolkit would be further enhanced by the development of inhibitors that can selectively target DAGLα or DAGLβ. Accordingly, even though studies with genetically disrupted mice[13,14,17] would indicate that the most of the lipid changes caused by DAGL inhibitors in the brain are due to blockade of DAGLα, in the pharmacological experiments a contribution from DAGLβ cannot excluded at this stage, especially when evaluating the neuroinflammatory effects of DAGL inhibitors. Indeed, it has been found in other studies that DAGLβ$^{-/-}$ mice also show attenuated LPS-induced anapyrexia, possibly due to functions performed by DAGLβ specifically in microglia.[58]

The short half-life of DAGLα also presents some challenges for the current inhibitor described in this chapter, since it need to be administered to mice at relatively high doses (50 mg/kg) to maintain complete target engagement over a prolonged (> 8 h) period of time. Improving the pharmacokinetic properties of DAGLα inhibitors would thus benefit pharmacological studies aimed at studying prolonged inactivation of DAGLα *in vivo*. From a translational perspective, it will be interesting to determine which of the many phenotypes observed in DAGLα$^{-/-}$ mice are recapitulated in animals treated with DAGL inhibitors. The DAGLα$^{-/-}$ mice show reduced body weight due to hypophagia and, in this regard, resemble animals with genetic or pharmacological disruption of the CB_1R.[15] Humans treated with CB_1R antagonists/inverse agonists likewise exhibit weight loss, but these drugs were ultimately removed from the clinic due to neuropsychiatric side effects.[59] DAGLα$^{-/-}$ mice also display heightened anxiety-related behaviors that can be normalized, along with partial restoration of brain 2-AG content, by treatment with an MAGL inhibitor.[17] Thus, the potential clinical utility of DAGL inhibitors for obesity or other disorders[60-62] may depend on whether a therapeutic window can be established within which partial reductions in endocannabinoid signaling are found to produce beneficial effects while minimizing untoward neurological outcomes. The DAGL inhibitors reported herein, which produce a graded, dose-dependent blockade of 2-AG production in the CNS, provide a first opportunity to experimentally investigate these important questions.

Experimental section

Chemistry

General materials: All of reactions were performed using oven or flame-dried glassware and dry solvents. Reagents were purchased from Sigma Aldrich, Acros and Merck and used without further purification unless noted otherwise. All moisture sensitive reactions were performed under an argon atmosphere. Traces of water were removed from starting compounds by co-evaporation with toluene. ^{1}H-and ^{13}C-NMR spectra were recorded on a Bruker AV 400 MHz spectrometer at 400 (^{1}H) and 101 (^{13}C) MHz, or on a Bruker DMX-600 spectrometer 600 (^{1}H) and 150 (^{13}C) MHz using $CDCl_3$, or CD_3OD solvent, unless stated otherwise. Chemical shift values are reported in ppm with tetramethylsilane or solvent resonance as the internal standard ($CHCl_3$, δ

7.26 for ^{1}H, δ 77.16 for ^{13}C). Data are reported as follows: chemical shifts (δ), multiplicity (s = singlet, d = doublet, dd = double doublet, td = triple doublet, t = triplet, m = multiplet, br = broad), coupling constants *J* (Hz), and integration. High-resolution mass spectra (HRMS) were recorded by direct injection (2 µL of a 2 µM solution in water/acetonitrile 50/50 (v/v) and 0.1% formic acid) on a mass spectrometer (Thermo Finnigan LTQ orbitrap) equipped with an electrospray ion source in positive mode (source voltage 3.5 kV, sheath gas flow 10, capillary temperature 250 ^{o}C) with resolution R = 60,000 at m/z 400 (mass range m/z = 150-2,000) and dioctylphthalate (m/z = 391.28428) as a "lock mass". The high resolution mass spectrometer was calibrated prior to measurements with a calibration mixture (Thermo Finnigan). LC-MS analysis was performed on a Finnigan Surveyor HPLC system with a Gemmi C_{18} 50x4.60 mm column (detection at 200-600 nm), coupled to a Finnigan LCQ Adantage Max mass spectrometer with ESI. The applied buffers were H_2O, MeCN and 1.0% TFA in H_2O (0.1% TFA end concentration). Flash chromatography was performed using SiliCycle silica gel type SilicaFlash P60 (230 – 400 mesh). TLC analysis was performed on Merck silica gel 60/Kieselguhr F254, 0.25 mm. Compounds were visualized using either Seebach's reagent (a mixture of phosphomolybdic acid (25 g), cerium (IV) sulfate (7.5 g), H_2O (500 mL) and H_2SO_4 (25 mL)) or a $KMnO_4$ stain (K_2CO_3 (40 g), $KMnO_4$ (6 g), H_2O (600 mL) and 10% NaOH (5 mL)).

Synthesis of ABP-DH379: Bodipy-Azide **1**[63] (14.2 mg, 0.030 mmol) and DH376 (15.0 mg, 0.028 mmol), were dissolved in degassed DCM/H_2O (1:1, 2 mL) and sodium ascorbate (6.57 mg, 0.033 mmol) and $CuSO_4$ (3.45 mg, 0.014 mmol) were added. The resulting mixture was stirred vigorously for two hours, after which TLC indicated completed conversion of the reaction. The solvents were evaporated *in vacuo* and the residue was taken up in DCM and purified by silica gel column chromatography (ethyl acetate with 1% AcOH) yielding probe DH379 (9.0 mg, 0.009 mmol, 32%) as a purple solid. ^{1}H NMR (600 MHz, $CDCl_3$) δ 7.85 (br s, 2H), 7.43 (br s, 11H), 7.09 – 6.91 (m, 8H), 6.51 (br s, 1H), 4.73 (br s, 2H), 3.94 (br s, 2H), 3.67 (br s, 1H), 3.53 (br s, 1H), 3.04 (br s, 2H), 2.74 (br s, 3H), 2.51 (br s, 5H), 2.21 (br s, 3H), 1.72 (br s, 3H), 1.25 (br s, 5H), 0.92 – 0.84 (m, 2H); ^{13}C NMR (151 MHz, $CDCl_3$) δ 176.20, 162.81 (d, *J* = 242 Hz), 159.61, 159.12, 155.38, 148.95, 141.55, 141.14, 140.72, 140.16, 137.78, 135.10, 134.51, 130.94, 130.05, 129.56, 129.24, 128.76, 128.14, 126.84, 126.22, 123.23, 118.45, 115.19 (d, *J* = 18 Hz), 114.25, 76.24, 73.67, 64.09, 54.22, 51.04, 48.95, 46.61, 35.69, 29.84, 26.55, 24.64, 22.83, 14.27, 13.34, 9.83; HRMS(m/z):$[M+H]^+$ calcd. for $C_{54}H_{52}BF_4N_9O_6$, 1010.41515; found 1010.41550.

Materials of chemical biological assays

Fluorophosphonate (FP)-rhodamine, FP-biotin and HT-01 were synthesized according to a previously described protocol.[64-68] FP-rhodamine is also commercially available at Thermo Fischer Scientific. All deuterated lipid standards and substrates were purchased from Cayman Chemicals.

Molecular cloning and recombinant expression

DAGLα/β plasmids: For the preparation of the different constructs, full length human cDNA was purchased from Source Bioscience and mouse cDNA was purchased from Open Biosystems, and were cloned into mammalian expression vector pcDNA3.1, containing genes for ampicillin and neomycin resistance. DAGLα/β constructs were obtained as reported previously.[68,69] For proteins containing a FLAG-tag, a FLAG-linker was made from primers and cloned into the vector at the C-terminus of hDAGLα or hDAGLβ. Two step PCR mutagenesis was performed to substitute the active site serine for an alanine in the hDAGLβ-FLAG, to obtain hDAGLβ-S443A-FLAG. Plasmids were isolated from transformed XL-10 Z-competent cells (Maxi Prep, Qiagen) and verified by Sanger sequencing (BaseClear).

Cell culture and membrane preparation: Cell culture and membrane preparation were performed as previously described.[68] In brief, HEK293T cells were grown in DMEM with stable glutamine and phenol red (PAA), 10% New Born Calf serum, penicillin and streptomycin. Cells were passaged every 2-3 days by resuspending in medium and seeding them to appropriate confluence. Membranes were prepared from transiently transfected HEK293T cells. One day prior to transfection 10^7 cells were seeded in a 15 cm petri dish. Cells were transfected by the addition of a 3:1 mixture of polyethyleneimine (60 µg) and plasmid DNA (20 µg) in 2 mL serum free medium. The medium was refreshed after 24 h, and after 72h the cells were harvested by suspending them in 20 mL medium. The suspension was centrifuged for 10 min at 1000 rpm, and the supernatant was removed. The cell pellet was stored at -80 ^{o}C until use.

Cell pellets were thawed on ice and suspended in lysis buffer A (20 mM HEPES, 2 mM DTT, 0.25 M sucrose, 1 mM $MgCl_2$, 1x protease inhibitor cocktail (Roche cOmplete EDTA free), 25U/µL Benzonase). The suspension was homogenized by polytrone (3 × 7 sec) and incubated for 30 min on ice. The suspension was subjected to ultracentrifugation (100.000 × g, 30 min, 4 ^{o}C, Beckman Coulter, Type Ti70 rotor) to yield the cytosolic fraction in the supernatant and the membrane fraction as a pellet. The pellet was resuspended in lysis buffer B (20 mM HEPES, 2 mM DTT, 1x protease inhibitor cocktail (Roche cOmplete EDTA free)). The protein concentration was determined with Quick Start Bradford assay (Biorad). The protein fractions were diluted to a total protein concentration of 1 mg/mL and stored in small aliquots at -80 ^{o}C until use.

Enzyme activity assays and IC_{50} measurements

PNP-butyrate DAGL activity assay: The para-nitrophenylbutyrate (PNP-butyrate) substrate assay was performed with hDAGLα as reported previously.[68] In brief, this assay is based on the hydrolysis of PNP-butyrate by membrane preparations from HEK293T cells transiently transfected with hDAGLα. Reactions were performed in 50 mM pH 7.2 HEPES buffer with 0.05 µg/µL final protein concentration to which PNP-butyrate substrate was added (5.0 µL in DMSO) to a final substrate

concentration of 300 µM. For the progression curve, after 135 minutes, another equal amount of substrate (5.0 µL, 12 mM) was added.

Natural substrate-based fluorescence assay (DAGLα/β): The natural DAG substrate assay was performed as reported previously.[70] Standard assay conditions: 0.2 U/mL glycerol kinase (GK), glycerol-3-phosphate oxidase (GPO) and horseradish peroxidase (HRP), 0.125 mM ATP, 10 µM Amplifu™Red, 5% DMSO in a total volume of 200 µL. The assay additionally contained 5 µg/mL MAGL-overexpressing membranes, 100 µM SAG and 0.0075% (w/v) Triton X-100, with a final protein concentration of 50 µg/mL. The mDAGLβ assay was performed as the hDAGLα assay, but assay buffer was supplemented with 5 mM $CaCl_2$ and the SAG concentration was 75 µM.

Activity based protein profiling on transiently transfected HEK293T cells

HEK293T cells were transfected with hDAGLα-FLAG or hDAGLα-S472A-FLAG, hDAGLβ-FLAG or hDAGLβ-S443A-FLAG and the membranes were isolated following a protocol reported previously.[68] For DAGLα ABPP assays the membrane proteome (1 mg/mL, 20 µL) was incubated at rt with vehicle (DMSO) or inhibitor in 0.5 µL DMSO for 30 min. The sample was subsequently treated for 15 min with 1µM (final concentration) ABP DH379 or 500 nM (final concentration) TAMRA-FP. The reactions were quenched with 10 µL 3 × Laemmli sample buffer (final concentrations: 60 mM Tris-Cl pH 6.8, 2% (w/v) SDS, 10% (v/v) glycerol, 5% (v/v) β-mercaptoethanol, 0.01% (v/v) bromophenol blue). The samples were directly loaded and resolved on SDS page gel (10 % acrylamide). The gels were scanned using a ChemiDoc MP system (Cy3 settings, 605/50 filter).

Western blot

Western blot procedure was performed as reported previously.[68] In brief, proteins were transferred from gel to a polyvinyldifluoride membrane using a Trans-Blot® Turbo (BioRad). FLAG-tagged enzymes were stained using rabbit anti-FLAG as primary antibody, and goat-anti-rabbit HRP as secondary antibody. The blot was developed in the dark using a 10 mL luminal solution, 100 µL ECL enhancer and 3 µL H_2O_2. Chemiluminescence was visualized using a ChemiDoc XRS (BioRad).

Size exclusion experiment

Membrane proteome (1 mg/mL, 343 µL) from transfected HEK293T cells was incubated with DMSO or inhibitor in 7.0 µL DMSO for 30 min at r.t. and subsequently the protein-inhibitor complex was loaded on the size exclusion column (Zeba spin desalting columns, 2 mL). After centrifugation (1000g, 2 min) the sample was collected, and the column flushed 3 times by centrifugation (1000g, 2 min) with 1 mL of storage buffer B (20 mM HEPES, pH 7.2; 2 mM DTT). After size exclusion, 19.5 µL of protein-inhibitor complex were used to perform ABPP. The rest of the sample was

reloaded onto the column, and centrifugation of sample, flushing of sample and collection of 19.5 µL of sample for ABPP, were repeated several times.

ABPP inhibitor activity measurements

The percentage of activity remaining was determined by measuring the integrated optical intensity of the fluorescent protein bands using image lab 4.1. The relative intensity was compared to the vehicle treated proteins, which were set to 100%. IC_{50} and IC_{80} values were determined by plotting a log(inhibitor) vs. normalized response (Variable slope) dose-response curve generated using Prism software (GraphPad).

Matings and genotyping of transgenic animals

All animal experiments were carried out in compliance with institutional animal protocols, and mice were housed on a normal 6AM/6PM light/dark phase with ad libitum access to water and food. C56Bl/6 mice were use in all inhibitor treatment studies. DAGLα$^{-/-}$ and DAGLβ$^{-/-}$[67] mice were generated by heterozygous matings and were in a homogeneous C57Bl/6 background. For these DAGL transgenic mice PCR genotyping of genomic tail DNA was performed using the following primers: DAGLα5'-tgagattggtatcaagacctttg-3', 5'-ccttgctcctgccgagaaagtatcc-3', and 5'- gaagaacaggtaaccaggaccat-3' (300-bp product in wild-type mice, 600-bp product in mice with the DAGLα null allele); DAGLβ 5'-aaggaggcaaagacagcaaagtgc-3', 5'-tatcctaggtgcagacagattgtgc-3', and 5'-aaatggcgttacttaagctagcttgc-3' (390-bp product in wild-type mice, 195-bp product in mice with the DAGLβ null allele).

Preparation of tissue proteomes

Mouse tissues were dounce homogenized in lysis buffer (20 mM HEPES, 250 mM sucrose, 2 mM DTT, 1 mM $MgCl_2$ with or without 25 U/mL benzonase) and incubated in ice for 5 min, followed by a low-speed spin (1,400−2.500 x g, 3 min, 4 °C) to remove debris. The membrane and cytosolic fractions were separated by ultracentrifugation (100,000 x *g*, 45 min, 4 °C) of the resulting homogenate lysate. After removal of the soluble supernatant, the membrane pellet was washed 1X with cold HEPES buffer (20 mM, with or without 2 mM DTT) followed by resuspension in cold HEPES buffer (20 mM, with or without 2 mM DTT) by pipetting. Total protein concentrations in membrane and soluble fractions were determined using the Bio-Rad DC protein assay kit. Samples were stored at -80 °C until further use.

Tissue profiling by gel-based competitive ABPP

Gel-based ABPP assays were performed as previously reported.[71] Cell or tissue proteomes were treated with either FP-rhodamine (1 µM or 500 nM final concentration), HT-01 (1 µM final concentration), or DH379 (1 µM final concentration). For HT-01and DH379 labeled samples, 2 mg/mL of proteome was used to enhance endogenous DAGL signals; 1 mg/mL proteome was used for labeling with FP-Rh. Probe labeling was carried out for 30 min at r.t. or 37 °C followed by addition of 4X

SDS-PAGE loading buffer to quench the reaction. After separation by SDS-PAGE (10% acrylamide), samples were visualized by in-gel fluorescence scanning using a ChemiDoc MP system.

Copper-catalyzed azide-alkyne cycloaddition (CuAAC or click) chemistry-ABPP

Mouse brain membrane proteomes from either naïve (in vitro) or inhibitor-treated (in vivo) mice were prepared for analysis as described in preparation of tissue proteome. Using previously developed methods,[72] Cyanine 5-Azide (Cy5−N_3) was conjugated to each alkyne probe for in-gel analysis. Briefly, $CuSO_4$ (1.0 µL/reaction, 100 mM in H_2O), THPTA (0.2 µL/reaction, 100 mM in H_2O), sodium ascorbate (0.6 µL/reaction, 1 M in H_2O [freshly prepared]), and Cy5−N_3 (0.2 µL/reaction, 0.4 mM in DMSO) were premixed. This click reagent mixture (2.0 µL total volume) was immediately added to each proteome (18 µL), and the reaction was stirred by briefly vortexing. After 30 min at room temperature, reactions were diluted with 4×SDS loading buffer (10 µL) and resolved by SDS-PAGE.

***In vivo* studies with DH376, DO34 and DO53**

The animal experiments were conducted in accordance with the guidelines of the Institutional Animal Care and Use Committee of The Scripps Research Institute and the ethical committee of Leiden University (DEC#14137). In vivo studies with DH376, DO34 and DO53 were conducted in C57BL/6 mice. Mice were injected with DH376 i.p. in 18:1:1 (v/v/v) solution of saline/ethanol/PEG40 (ethoxylated castor oil, 10 µL/g body weight of mouse). For dose-response studies, mice were treated with varying doses of compounds for 4 h, anesthetized with isoflurane, and euthanized by cervical dislocation. For time-course studies, mice were treated with 50 mg/kg body weight of compound and euthanized after the indicated times. LPS-induced neuroinflammation studies were performed as previously described[73]. Mice were pretreated with compounds i.p. in vehicle of 18:1:1 (v/v/v) solution of saline/ethanol/PEG40 (ethoxylated castor oil, 10 µL/g body weight of mouse) and incubated for 1-1.5 h. After the pretreatment, mice were treated with 20 mg/kg body weight of LPS i.p. in saline (10 µl/g body weight of mouse) and euthanized after 6 h.

Sample preparation and targeted LC/MS metabolite profiling

Mice were anesthetized by isoflurane and euthanized by decapitation. Brain tissues were harvested, and immediately frozen in liquid nitrogen. Tissues were then dounce-homogenized in 8 ml of 2:1:1 $CHCl_3$/MeOH/PBS containing the internal standard mix (1 nmol of 2-arachidonoylglycerol-d5 (2-AG-d_5), arachidonic acid-d8 (AA-d_8), anandamide-d5 (AEA-d_4), 1-stearoyl-2-arachidonoyl-sn-glycerol-d8 (SAG-d_8), prostaglandin E2-d9 (PGE2-d_9) (Cayman Chemical), 1-heptadecanoyl-2-hydroxy-sn-glycero-3-phosphocholine (LysoPC), 1,2-diheptadecanoyl-sn-glycero-3-phosphocholine (PC), 1,2-diheptadecanoyl-sn-glycero-3-phosphoethanolamine (PE), 1-(10Z-heptadecenoyl)-2-hydroxy-sn-glycero-3-[phosphor-L-serine] (LysoPS),

1,2-diheptadecanoyl-sn-glycero-3-phospho-L-serine (PS), 1,2-diheptadecanoyl-sn-glycero-3-[phosphor-rac-(1-glycerol)] (PG), 1-heptadecanoyl-2-arachidonoyl-sn-glycero-3-phospho(1'-myo-inositol) (PI) (Avanti Polar Lipids) and 1,2-dioleoyl-sn-glycero-3-phospho (N-nonadecenoyl) ethanolamine[74] (NAPE)). Homogenates were centrifuged at 1,400 x *g* for 3 min to separate the two phases. The organic phase (bottom) was removed, 20 µL of formic acid was added to acidify the aqueous homogenate and $CHCl_3$ was added to make up 8 mL volume. The mixture was vortexed and separated using centrifugation as described above. Both the organic extracts were pooled and dried under a stream of N_2. The metabolomes were resolubilized in 480 µL of 2:1 $CHCl_3$/MeOH, and 10 µL were used for the targeted LC/MS analysis.

Metabolites analyzed in this study were quantified using LC/MS–based multiple reaction monitoring (MRM) methods (Agilent Technologies 6460 Triple Quad). Liquid chromatography (LC) separation was achieved using a Gemini reverse-phase C18 column (50 x 4.6 mm with 5 µm diameter particles, Phenomonex) along with a pre-column (C18, 3.5 µm, 2 mm x 20 mm). For analysis of diacylglycerols (DAGs) a Luna C5 column (50 x 4.60 mm with 5 µm diameter particles) was used. Mobile phase A was made of 95:5 (v/v) H_2O:MeOH, and mobile phase B was composed of 60:35:5 (v/v/v) *i*-PrOH:MeOH:H_2O. Ammonium hydroxide (0.1%) and formic acid (0.1%) was included to assist in ion formation in negative and positive ionization modes, respectively. For analysis of DAGs, 5 mM ammonium formate was also used in addition to 0.1% formic acid to assist in positive ionization and NH_4^+ adduct formation. MS analysis was performed with an ESI source in scanning mode from m/z = 50 – 1,200, capillary voltage set to 3.5 kV, and the fragmentor voltage set to 100 V. The drying gas temperature was set to 300 °C, drying gas flow rate was 11 L/min, and nebulizer pressure was 35 psi. The parameters (MS) used for MRM to measure the indicated metabolites are summarized in Table 2. Endogenous lipids were quantified by measuring the area under the peak in comparison with the appropriate unnatural internal standard and normalizing for tissue weight.

ABPP-reductive dimethylation (ReDiMe) sample preparation and analysis

For the ABPP-ReDiMe samples, proteomes (2 mg/mL in 20 mM HEPES buffer) were labeled with FP-biotin (10 µM) for 1h at rt. After labeling, the proteomes were denatured and precipitated using 4:1 MeOH/$CHCl_3$, resuspended in 0.5 mL of 6 M urea in PBS with 0.4% SDS, reduced using Tris(2-carboxyethyl)phosphine (TCEP, 20 mM)/K_2CO_3 (60 mM) for 30 min at 37 °C and then alkylated using iodoacetamide (40 mM) for 30 min at 25 °C in the dark. The biotinylated proteins were enriched with PBS-washed streptavidn-agarose beads (100 µL; Thermo) by shaking at rt for 1.5 h in PBS with 2% SDS to final volume of 5.5 mL. The beads were washed sequentially with 15 mL PBS with 1% SDS (3×), 15 mLPBS (3×) and 15 mL DI H_2O (3×). On-bead digestion was performed using sequence-grade trypsin (1.5 µg; Promega) in 2 M urea in triethylammonium bicarbonate buffer (100 mM, 200 µL) with 1 mM $CaCl_2$ for 12–16 h at 37 °C with constant shaking. Reductive dimethylation was performed as

previously described.[75,76] Briefly, either ^{13}C-labeled deuterated formaldehyde (heavy) or formaldehyde (light) was added to each sample (0.2%) followed by addition of sodium cyanoborohydride (27 mM). Following a 2h incubation period at room temperature, the reaction was quenched by addition of NH_4OH (0.2 %) and formic acid (8 %). The samples were then combined and analyzed by LC/MS analysis.

MS and data analysis

MS was performed using an Orbitrap Velos mass spectrometer following previously described protocols.[77, 78] Peptides were eluted using a five-step multidimensional LC/MS [MudPIT[79]] protocol (using 0%, 25%, 50%, 80% and 100% salt bumps of 500 mM aqueous ammonium acetate, followed by an increasing gradient of aqueous acetonitrile and 0.1% formic acid in each step). For all samples, data were collected in data-dependent acquisition mode over a range from 400–1,800 *m*/*z*. Each full scan was followed by up to 30 fragmentation events for experiments using Orbitrap Velos instruments. Dynamic exclusion was enabled (repeat count of 1, exclusion duration of 20 s) for all experiments. The data were searched using the ProLuCID algorithm against a mouse reverse-concatenated nonredundant (gene-centric) FASTA database that was assembled from the Uniprot database. ProLuCID searches specified static modification of cysteine residues (+57.0215 *m*/*z*; iodoacetamide alkylation) and required peptides to contain at least one tryptic terminus. Each data set was independently searched with light and heavy parameter files; for the light search, static modifications on lysine (+ 28.0313 *m*/*z*) and N termini (+ 28.0313 *m*/*z*) were specified; for the heavy search, static modifications on lysine (+ 34.06312 *m*/*z*) and N termini (+ 34.06312 *m*/*z*) were specified. The resulting matched MS2 spectra were assembled into protein identifications, then filtered using DTASelect (version 2.0.47). Peptides were restricted to a specified false positive rate of <1%. ReDiMe ratios were quantified using in-house CIMAGE[80] software. Briefly, extracted MS1 ion chromatograms (± 10 ppm) from both 'light' and 'heavy' target peptide masses (*m/z*) were generated using a retention time window (± 10 min) centered on the time when the peptide ion was selected for MS/MS fragmentation, and subsequently identified. Next, the ratios of the peak areas under the light and heavy signals (signal-to-noise ratio > 2.5) are calculated. Computational filters used to ensure that the correct peak-pair is used for quantification include a co-elution correlation score filter ($R2 \geq 0.8$), removing target peptides with bad co-elution profile, and an 'envelope correlation score' filter ($R2 > 0.8$) that eliminates target peptides whose predicted pattern of the isotopic envelope distribution does not match the experimentally observed high-resolution MS1 spectrum. Also, peptides detected as singletons, where only the heavy or light isotopically labeled peptide was detected and sequenced, but which passed all other filtering parameters, were given a standard ratio of 20, which is the maximum ReDiMe ratio reported here.

Cytokine measurements

Cytokines were measured using mouse DuoSet® ELISA development kit (R&D Systems). Brains were homogenized in phosphate-buffered saline with 1 x protease

inhibitor cocktail (Roche). The supernatant from a 1400 x g centrifugation of the homogenate was then centrifuged at 100,000 x g for 45 min. The supernatant from this centrifugation (the mouse brain soluble proteome) was used in the assay.

Slice preparation

C57BL/6J mice of either sex were anaesthetized by isoflurane inhalation and decapitated. Parasagittal slices (250 µm thick) were cut from the cerebellar vermis of 10- to 14-day-old mice, and transverse slices (250 µm thick) were cut from the hippocampus of 20- to 30-day-old mice, as it has been described.[81,82] Slices were prepared at 4-6°C in a sucrose-based solution containing (in mM): 78 NaCl, 68 sucrose, 26 $NaHCO_3$, 2.5 KCl, 1.25 NaH_2PO_4, 2 $CaCl_2$, 2 $MgCl_2$ and 25 glucose. Slices were incubated for 30-40 min in sucrose solution and then transferred and stored in the artificial cerebrospinal fluid (ACSF) containing (in mM): 119 NaCl, 2.5 KCl, 2.5 $CaCl_2$, 1 $MgCl_2$, 1.25 NaH_2PO_4, 26 $NaHCO_3$, and 10 glucose. All solutions were saturated with 95% O_2 and 5% CO_2.

Electrophysiology

Whole-cell recordings were made using patch clamp amplifier Multiclamp 700B under infrared-DIC microscopy. Data acquisition and analysis were performed using DigiData 1440A digitizer and analysis software pClamp 10 (Molecular Devices). Signals were filtered at 2 kHz and sampled at 10 kHz. Whole-cell voltage-clamp recordings were made from cerebellar Purkinje cells (PCs) and hippocampal CA1 pyramidal neurons as described previously.[81,82] Excitatory postsynaptic currents (EPSCs) were recorded from cerebellar Purkinje cells (PCs), parallel fibers (PFs) were stimulated with a bipolar tungsten stimulation electrode (WPI) that was placed in the molecular layer. PF-EPSCs showed graded responses and exhibited paired-pulse facilitation (30-50 ms intervals).[83] $GABA_A$ receptor blocker picrotoxin (50 µM) and a low concentration (1 µM) of AMPA receptor antagonist 6-cyano-7-nitroquinoxaline-2,3-dione (CNQX) was present in the ACSF. Glass pipettes (3-5 MΩ) were filled with an internal solution containing (in mM): 140 cesium methanesulfonate, 10 CsCl, 2 QX-314, 10 HEPES, 0.2 EGTA, 2 $MgCl_2$, 4 Mg-ATP, and 0.3 Na_2GTP (pH 7.2 with CsOH). EPSCs were evoked by electrical stimulation at 4 s intervals. DSE was induced by a brief depolarization (1 s from -70 mV to 0 mV).

Inhibitory postsynaptic currents (IPSCs) were recorded from CA1 pyramidal neurons in hippocampal slices. A bipolar tungsten stimulation electrode was placed in the stratum radiatum of the CA1 region to evoke IPSCs. AMPA receptor antagonist CNQX (20 µM) and NMDA receptor antagonist D-2-amino-5-phosphonovaleric acid (D-AP-5, 20 µM) were present in the ACSF. The pipettes were filled with an internal solution containing (in mM): 100 K-gluconate, 50 KCl, 0.1 $CaCl_2$, 1 EGTA-Na_4, 2 $MgCl_2$, 2 Mg-ATP, 0.3 Na_2GTP, and 10 HEPES at pH 7.2 (with KOH). To induce DSI, the CA1 pyramidal neurons were depolarized from -70 mV to 0 mV for 5 s, and IPSCs were evoked at 4 s intervals. All recordings were performed at 32 ± 1°C by using an

automatic temperature controller. DAGL inhibitors and control compounds were dissolved in DMSO and the final concentration of DMSO in the ACSF is ≤0.1%.

Anapyrexia study

Core body temperature was measured by radiotelemetry as previously described.[84-87] Briefly, mice were anesthetized with isofluorane (induction 3-5%, maintenance 1-1.5%) and surgically implanted with radiotelemetry devices (TA-F20, Data Sciences, St. Paul, MN) into the peritoneal cavity for core body temperature (CBT) and locomotor activity (LA) evaluation. Following surgical implantation and appropriate wound closure, the animals were allowed to recover for 2 weeks and then subjected to telemetry recordings. Mice were individually housed in a Plexiglas cage in a room maintained at 25 ± 0.5°C. The cages were positioned onto the receiver plates (RPC-1; Data Sciences) and radio signal reporting CBT and LA information from the implanted transmitter was recorded continuously with a fully automated data acquisition system (Dataquest ART, Data Sciences, St. Paul, MN). Access to food and water was ad libitum and the light:dark cycle was of 12h:12h. Anapyrexia was induced by intraperitoneal injection of *Bacterial lipopolysaccharides (LPS)* (0127:B8, Sigma, St. Louis, MO) at a dose of 10 mg/kg in saline. DH376, DO34 and DO53 were injected intraperitoneally at a dose of 50 mg/kg in emulfor:ethanol:saline 1:1:18 2h before injection of LPS. Saline and emulfor:ethanol:saline were used as vehicle.

Data analysis and statistics

Data are shown as the mean ± SEM. A Student's t test (unpaired, two-tailed) was used to determine differences between two groups. Data that included more than two groups or two factors were analyzed by one-way or two-way ANOVA, respectively, with post hoc Sidak's multiple comparisons test. All statistical analyses were conducted using Excel or GraphPad Prism version 6, and a P value less than 0.05 was considered significant throughout unless indicated otherwise. For brain lipid profiling study for DH376 -, DO34- and DO53-treated mice and DAGLα$^{-/-}$ mice (Table 2), Benjamini Hochberg correction (10 % false discovery rate) was applied. Post-correction p values < 0.007 were designated as significant and are marked in red. P values between 0.007 and 0.05 were also listed in blue, with remaining p values designated as NS (not significant). For electrophysiology data, DSE and DSI were analyzed as described in the previous studies.[81, 82]

Radioligand binding assay

Materials: [^{3}H]CP55940 (specific activity 141.2 Ci/mmol) and GF-C filters were purchased from Perkin Elmer (Waltham, MA). Bicinchoninic acid (BCA) and BCA protein assay reagent were obtained from Pierce Chemical Company (Rochford, IL). The PathHunter® CHO-K1 CNR1 β-Arrestin Cell Line (catalog number 93-0959C2) and the PathHunter® CHO-K1 CNR2 β-Arrestin Cell Line (catalog number 93-0706C2), stably expressing the hCB_1 receptor (CHOK1hCB_1_bgal) or hCB_2 receptor (CHOK1hCB_2_bgal) respectively, was obtained from DiscoveRx.

Cell culture and membrane preparation: CHOK1hCB_1_bgal and CHOK1hCB_2_bgal cells were cultured in Ham's F12 Nutrient Mixture supplemented with 10% fetal calf serum, 1 mM glutamine, 50 µg/mL penicillin, 50 µg/mL streptomycin, 300 mg/mL hygromycin and 800 µg/mL geneticin in a humidified atmosphere at 37 °C and 5% CO_2. Cells were subcultured twice a week at a ratio of 1:20 on 10 cm plates by trypsinization. For membrane preparation the cells were subcultured 1:10 and transferred to large 15-cm diameter plates. Membrane fractions were prepared exactly as described before.[88]

[^{3}H]CP55940 radioligand binding assay: [^{3}H]CP55940 binding assays to determine the cannabinoid CB_1 and CB_2 receptor binding affinity were performed as follows: Ligands of interest were incubated at 30 °C for 1 hr with membrane aliquots containing 5 µg CHOK1hCB_1_bgal membrane protein or 1 µg (CHOK1hCB_2_bgal) in 100 µL assay buffer (50 mM Tris–HCl, 5 mM $MgCl_2$, 0.1% BSA, pH 7.4) with [^{3}H]CP55940 in a concentration of ~1.5 nM (CB_2 receptor) or ~3.5 nM (CB_1 receptor) per assay point. Non-specific binding was determined in the presence of 10 µM Rimonabant (CB_1 receptor) or 10 µM AM630 (CB_2 receptor). Filtration was performed on GF/C filters, presoaked for 30 min with 0.25% polyethylenimine, using a Brandel harvester. Filter-bound radioactivity was determined in a β-counter. The mean % of specific binding for CB_1 and CB_2 receptors were 36 ± 4% and 38 ± 42% for 6-12 experiments.

Supporting Figures

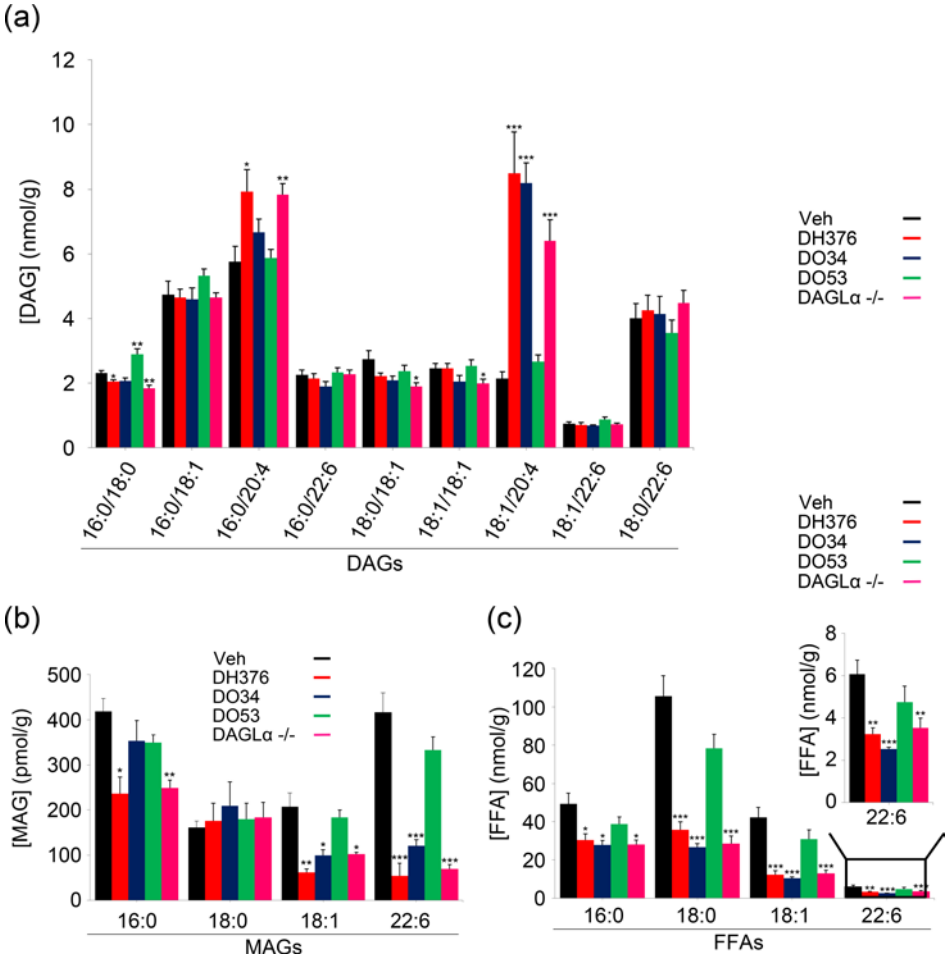

Figure S1. Additional brain lipid profiles in mice treated with DAGL inhibitors. Quantification of DAG (a), MAG (b), FFA (c) in brain tissue from mice treated with vehicle or DH376, DO34, and DO53 (50 mg/kg, i.p., 4 h). Lipid profiles from DAGLα$^{-/-}$ mice are shown for comparison. Data represent average values ± SEM; n = 4-6 mice per group. *p < 0.05; **p < 0.01; ***p < 0.001 for inhibitor-treated DAGLα$^{+/+}$ mice or DAGLα$^{-/-}$ mice vs. vehicle-treated DAGLα$^{+/+}$ mice.

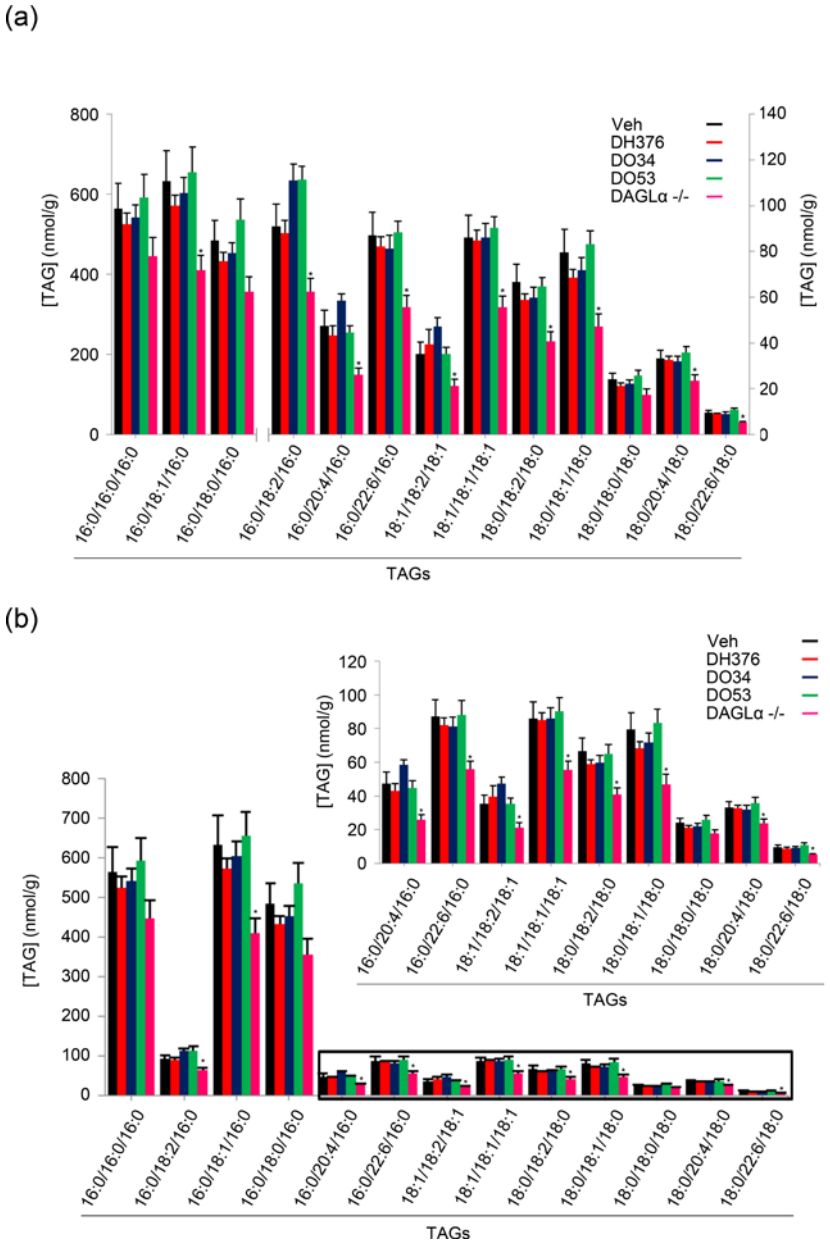

Figure S2. Additional brain lipid profiles in mice treated with DAGL inhibitors. Quantification of TAG in brain tissue from mice treated with vehicle or DH376, DO34, and DO53 (50 mg/kg, i.p., 4 h). Lipid profiles from DAGLα$^{-/-}$ mice are shown for comparison. Data represent average values ± SEM; n = 4-6 mice per group. *p < 0.05; **p < 0.01; ***p < 0.001 for inhibitor-treated DAGLα$^{+/+}$ mice or DAGLα$^{-/-}$ mice vs. vehicle-treated DAGLα$^{+/+}$ mice.

References

1. Brady, S.; Siegel, G.; Albers, R. W.; Price, D. *Basic Neurochemistry*. 8 ed.; Academic Press: Waltham, MA, 2012; p 235-389.
2. Yung, Y. C.; Stoddard, N. C.; Mirendil, H.; Chun, J. Lysophosphatidic acid signaling in the nervous system. *Neuron* **2015,** 85, 669-682.
3. Choi, J. W.; Chun, J. Lysophospholipids and their receptors in the central nervous system. *Biochimica et Biophysica acta* **2013,** 1831, 20-32.
4. Katona, I.; Freund, T. F. Endocannabinoid signaling as a synaptic circuit breaker in neurological disease. *Nature Medicine* **2008,** 14, 923-930.
5. Cimino, P. J.; Keene, C. D.; Breyer, R. M.; Montine, K. S.; Montine, T. J. Therapeutic targets in prostaglandin E2 signaling for neurologic disease. *Current MedicinalCchemistry* **2008,** 15, 1863-1869.
6. Bryan, L.; Kordula, T.; Spiegel, S.; Milstien, S. Regulation and functions of sphingosine kinases in the brain. *Biochimica et Biophysica acta* **2008,** 1781, 459-466.
7. Choi, S. H.; Aid, S.; Bosetti, F. The distinct roles of cyclooxygenase-1 and -2 in neuroinflammation: implications for translational research. *Trends in Pharmacological Sciences* **2009,** 30, 174-181.
8. Reisenberg, M.; Singh, P. K.; Williams, G.; Doherty, P. The diacylglycerol lipases: structure, regulation and roles in and beyond endocannabinoid signalling. *Philosophical Transactions of the Royal Society of London. Series B, Biological Sciences* **2012,** 367, 3264-3275.
9. Murataeva, N.; Straiker, A.; Mackie, K. Parsing the players: 2-arachidonoylglycerol synthesis and degradation in the CNS. *British Journal of Pharmacology* **2014,** 171, 1379-1391.
10. Bisogno, T.; Howell, F.; WIlliams, G.; Minassi, A.; Cascio, M. G.; Ligresti, A.; Matias, I.; Schiano-Moriello, A.; Paul, P.; Williams, E. J.; Gangadharan, U.; Hobbs, C.; Di Marzo, V.; Doherty, P. Cloning of the first sn1-DAG lipases points to the spatial and temporal regulation of endocannabinoid signaling in the brain. *Journal of Cell Biology.* **2003,** 163, 463-468.
11. Mechoulam, R.; Ben-Shabat, S.; Hanus, L.; Ligumsky, M.; Kaminski, N. E.; Schatz, A. R.; Gopher, A.; Almog, S.; Martin, B. R.; Compton, D. R. Identification of an endogenous 2-monoglyceride, present in canine gut, that binds cannabinoid receptors. *Biochemical Pharmacology* **1995,** 50, 83-90.
12. Sugiura, T.; Kondo, S.; Sukagawa, A.; Nakane, S.; Shinoda, A.; Itoh, K.; Yamashita, A.; Waku, K. 2-Arachidonylglycerol: a possible endogenous cannabinoid receptor ligand in brain. *Biochemical Biophysical Research Communications* **1995,** 215, 89-97.
13. Gao, Y.; Vasilyev, D. V.; Goncalves, M. B.; Howell, F. V.; Hobbs, C.; Reisenberg, M.; Shen, R.; Zhang, M. Y.; Strassle, B. W.; Lu, P.; Mark, L.; Piesla, M. J.; Deng, K.; Kouranova, E. V.; Ring, R. H.; Whiteside, G. T.; Bates, B.; Walsh, F. S.; Williams, G.; Pangalos, M. N.; Samad, T. A.; Doherty, P. Loss of retrograde endocannabinoid signaling and reduced adult neurogenesis in diacylglycerol lipase knock-out mice. *The Journal of Neuroscience : the official Journal of the Society for Neuroscience* **2010,** 30, 2017-2024.

14. Tanimura, A.; Yamazaki, M.; Hashimotodani, Y.; Uchigashima, M.; Kawata, S.; Abe, M.; Kita, Y.; Hashimoto, K.; Shimizu, T.; Watanabe, M.; Sakimura, K.; Kano, M. The endocannabinoid 2-arachidonoylglycerol produced by diacylglycerol lipase alpha mediates retrograde suppression of synaptic transmission. *Neuron* **2010,** 65, 320-327.
15. Powell, D. R.; Gay, J. P.; Wilganowski, N.; Doree, D.; Savelieva, K. V.; Lanthorn, T. H.; Read, R.; Vogel, P.; Hansen, G. M.; Brommage, R.; Ding, Z. M.; Desai, U.; Zambrowicz, B. Diacylglycerol lipase alpha knockout mice demonstrate metabolic and behavioral phenotypes similar to those of cannabinoid receptor 1 knockout mice. *Frontiers in Endocrinology* **2015,** 6, 86.
16. Jenniches, I.; Ternes, S.; Albayram, O.; Otte, D. M.; Bach, K.; Bindila, L.; Michel, K.; Lutz, B.; Bilkei-Gorzo, A.; Zimmer, A. Anxiety, stress, and fear response in mice with reduced endocannabinoid levels. *Biological Psychiatry* **2015**.
17. Shonesy, B. C.; Bluett, R. J.; Ramikie, T. S.; Baldi, R.; Hermanson, D. J.; Kingsley, P. J.; Marnett, L. J.; Winder, D. G.; Colbran, R. J.; Patel, S. Genetic disruption of 2-arachidonoylglycerol synthesis reveals a key role for endocannabinoid signaling in anxiety modulation. *Cell Reports* **2014,** 9, 1644-1653.
18. Whatley, R. E.; Zimmerman, G. A.; McIntyre, T. M.; Prescott, S. M. Lipid metabolism and signal transduction in endothelial cells. *Progress in Lipid Research* **1990,** 29, 45-63.
19. Kohnz, R. A.; Nomura, D. K. Chemical approaches to therapeutically target the metabolism and signaling of the endocannabinoid 2-AG and eicosanoids. *Chemical Society Reviews* **2014,** 43, 6859-6869.
20. Kano, M.; Ohno-Shosaku, T.; Hashimotodani, Y.; Uchigashima, M.; Watanabe, M. Endocannabinoid-mediated control of synaptic transmission. *Physiological Reviews* **2009,** 89, 309-380.
21. Hashimotodani, Y.; Ohno-Shosaku, T.; Tanimura, A.; Kita, Y.; Sano, Y.; Shimizu, T.; Di Marzo, V.; Kano, M. Acute inhibition of diacylglycerol lipase blocks endocannabinoid-mediated retrograde signalling: evidence for on-demand biosynthesis of 2-arachidonoylglycerol. *The Journal of Physiology* **2013,** 591, 4765-4776.
22. Min, R.; Testa-Silva, G.; Heistek, T. S.; Canto, C. B.; Lodder, J. C.; Bisogno, T.; Di Marzo, V.; Brussaard, A. B.; Burnashev, N.; Mansvelder, H. D. Diacylglycerol lipase is not involved in depolarization-induced suppression of inhibition at unitary inhibitory connections in mouse hippocampus. *The Journal of Neuroscience : the official Journal of the Society for Neuroscience* **2010,** 30, 2710-2715.
23. Zhang, L.; Wang, M.; Bisogno, T.; Di Marzo, V.; Alger, B. E. Endocannabinoids generated by Ca2+ or by metabotropic glutamate receptors appear to arise from different pools of diacylglycerol lipase. *PloS one* **2011,** 6, e16305.
24. Bisogno, T.; Mahadevan, A.; Coccurello, R.; Chang, J. W.; Allara, M.; Chen, Y.; Giacovazzo, G.; Lichtman, A.; Cravatt, B.; Moles, A.; Di Marzo, V. A novel fluorophosphonate inhibitor of the biosynthesis of the endocannabinoid 2-arachidonoylglycerol with potential anti-obesity effects. *British Journal of Pharmacology* **2013,** 169, 784-793.
25. Baggelaar, M. P.; Chameau, P. J.; Kantae, V.; Hummel, J.; Hsu, K. L.; Janssen, F.; van der Wel, T.; Soethoudt, M.; Deng, H.; den Dulk, H.; Allara, M.; Florea, B. I.; Di Marzo, V.; Wadman, W. J.; Kruse, C. G.; Overkleeft, H. S.; Hankemeier, T.; Werkman, T. R.; Cravatt, B. F.; van der Stelt, M. Highly selective, reversible inhibitor identified by comparative

chemoproteomics modulates diacylglycerol lipase activity in neurons. *Journal of the American Chemical Society* **2015,** 137, 8851-8857.

26. Hoover, H. S.; Blankman, J. L.; Niessen, S.; Cravatt, B. F. Selectivity of inhibitors of endocannabinoid biosynthesis evaluated by activity-based protein profiling. *Bioorganic Medicinal Chemistry Letters* **2008**.
27. Hsu, K. L.; Tsuboi, K.; Adibekian, A.; Pugh, H.; Masuda, K.; Cravatt, B. F. DAGLbeta inhibition perturbs a lipid network involved in macrophage inflammatory responses. *Nature Chemical Biology* **2012,** 8, 999-1007.
28. Baggelaar, M. P.; Janssen, F. J.; van Esbroeck, A. C.; den Dulk, H.; Allara, M.; Hoogendoorn, S.; McGuire, R.; Florea, B. I.; Meeuwenoord, N.; van den Elst, H.; van der Marel, G. A.; Brouwer, J.; Di Marzo, V.; Overkleeft, H. S.; van der Stelt, M. Development of an activity-based probe and in silico design reveal highly selective inhibitors for diacylglycerol lipase-alpha in brain. *Angewandte Chemie International Edition* **2013,** 52, 12081-12085.
29. Niphakis, M. J.; Cravatt, B. F. Enzyme inhibitor discovery by activity-based protein profiling. *Annual Review Biochemistry* **2014,** 83, 341-377.
30. van der Wel, T.; Janssen, F. J.; Baggelaar, M. P.; Deng, H.; den Dulk, H.; Overkleeft, H. S.; van der Stelt, M. A natural substrate-based fluorescence assay for inhibitor screening on diacylglycerol lipase alpha. *Journal of Lipid Research* **2015,** 56, 927-935.
31. Rostovtsev, V. V.; Green, J. G.; Fokin, V. V.; Sharpless, K. B. A stepwise Huisgen cycloaddition process: copper(I)-catalyzed regioselective "ligation" of azides and terminal alkynes. *Angewandte Chemie International Edition* **2002,** 41, 2596-2599.
32. Patricelli, M. P.; Giang, D. K.; Stamp, L. M.; Burbaum, J. J. Direct visualization of serine hydrolase activities in complex proteome using fluorescent active site-directed probes. *Proteomics* **2001,** 1, 1067-1071.
33. Liu, Y. S.; Patricelli, M. P.; Cravatt, B. F. Activity-based protein profiling: The serine hydrolases. *Proceedings of the National Academy of Sciences of the United States of America* **1999,** 96, 14694-14699.
34. Wilson-Grady, J. T.; Haas, W.; Gygi, S. P. Quantitative comparison of the fasted and re-fed mouse liver phosphoproteomes using lower pH reductive dimethylation. *Methods* **2013,** 61, 277-286.
35. Baggelaar, M. P.; Chameau, P. J. P.; Kantae, V.; Hummel, J.; Hsu, K. L.; Janssen, F.; van der Wel, T.; Soethoudt, M.; Deng, H.; den Dulk, H.; Allara, M.; Florea, B. I.; Di Marzo, V.; Wadman, W. J.; Kruse, C. G.; Overkleeft, H. S.; Hankemeier, T.; Werkman, T. R.; Cravatt, B. F.; van der Stelt, M. Highly selective, inhibitor identified by comparative chemoproteomics modulates diacylglycerol lipase activity in neurons. *Journal of the American Chemical Society* **2015,** 137, 8851-8857.
36. Sugiura, T.; Kondo, S.; Sukagawa, A.; Nakane, S.; Shinoda, A.; Itoh, K.; Yamashita, A.; Waku, K. 2-Arachidonoylglycerol: a possible endogenous cannabinoid receptor ligand in brain. *Biochemical Biophysical Research Communications* **1995,** 215, 89-97.
37. Marignani, P. A.; Epand, R. M.; Sebaldt, R. J. Acyl chain dependence of diacylglycerol activation of protein kinase C activity in vitro. *Biochemical Biophysical Research Communications* **1996,** 225, 469-473.
38. Nomura, D. K.; Morrison, B. E.; Blankman, J. L.; Long, J. Z.; Kinsey, S. G.; Marcondes, M. C.; Ward, A. M.; Hahn, Y. K.; Lichtman, A. H.; Conti, B.; Cravatt, B. F. Endocannabinoid

hydrolysis generates brain prostaglandins that promote neuroinflammation. *Science* **2011,** 334, 809-813.

39. Kita, Y.; Yoshida, K.; Tokuoka, S. M.; Hamano, F.; Yamazaki, M.; Sakimura, K.; Kano, M.; Shimizu, T. Fever Is Mediated by Conversion of Endocannabinoid 2-arachidonoylglycerol to prostaglandin E2. *PloS one* **2015,** 10, e0133663.
40. Pasquarelli, N.; Porazik, C.; Hanselmann, J.; Weydt, P.; Ferger, B.; Witting, A. Comparative biochemical characterization of the monoacylglycerol lipase inhibitor KML29 in brain, spinal cord, liver, spleen, fat and muscle tissue. *Neuropharmacology* **2015,** 91, 148-156.
41. Viader, A.; Blankman, J. L.; Zhong, P.; Liu, X.; Schlosburg, J. E.; Joslyn, C. M.; Liu, Q. S.; Tomarchio, A. J.; Lichtman, A. H.; Selley, D. E.; Sim-Selley, L. J.; Cravatt, B. F. Metabolic interplay between astrocytes and neurons regulates endocannabinoid action. *Cell Reports* **2015,** 12, 798-808.
42. Steiner, A. A.; Molchanova, A. Y.; Dogan, M. D.; Patel, S.; Petervari, E.; Balasko, M.; Wanner, S. P.; Eales, J.; Oliveira, D. L.; Gavva, N. R.; Almeida, M. C.; Szekely, M.; Romanovsky, A. A. The hypothermic response to bacterial lipopolysaccharide critically depends on brain CB1, but not CB2 or TRPV1, receptors. *The Journal of Physiology* **2011,** 589, 2415-2431.
43. Nass, S. R.; Long, J. Z.; Schlosburg, J. E.; Cravatt, B. F.; Lichtman, A. H.; Kinsey, S. G. Endocannabinoid catabolic enzymes play differential roles in thermal homeostasis in response to environmental or immune challenge. *Journal of neuroimmune pharmacology : the official journal of the Society on NeuroImmune Pharmacology* **2015,** 10, 364-370.
44. Mechoulam, R.; Parker, L. A. The endocannabinoid system and the brain. *Annual Review of Psychology* **2013,** 64, 21-47.
45. Fowler, C. J. The potential of inhibitors of endocannabinoid metabolism as anxiolytic and antidepressive drugs--A practical view. *European Neuropsychopharmacology : the Journal of the European College of Neuropsychopharmacology* **2015,** 25, 749-762.
46. Blankman, J. L.; Cravatt, B. F. Chemical probes of endocannabinoid metabolism. *Pharmacological Reviews* **2013,** 65, 849-871.
47. Schlosburg, J. E.; Blankman, J. L.; Long, J. Z.; Nomura, D. K.; Pan, B.; Kinsey, S. G.; Nguyen, P. T.; Ramesh, D.; Booker, L.; Burston, J. J.; Thomas, E. A.; Selley, D. E.; Sim-Selley, L. J.; Liu, Q. S.; Lichtman, A. H.; Cravatt, B. F. Chronic monoacylglycerol lipase blockade causes functional antagonism of the endocannabinoid system. *Nature Neuroscience* **2010,** 13, 1113-1119.
48. Chanda, P. K.; Gao, Y.; Mark, L.; Btesh, J.; Strassle, B. W.; Lu, P.; Piesla, M. J.; Zhang, M. Y.; Bingham, B.; Uveges, A.; Kowal, D.; Garbe, D.; Kouranova, E. V.; Ring, R. H.; Bates, B.; Pangalos, M. N.; Kennedy, J. D.; Whiteside, G. T.; Samad, T. A. Monoacylglycerol lipase activity is a critical modulator of the tone and integrity of the endocannabinoid system. *Molecular Pharmacology* **2010,** 78, 996-1003.
49. Taschler, U.; Eichmann, T. O.; Radner, F. P.; Grabner, G. F.; Wolinski, H.; Storr, M.; Lass, A.; Schicho, R.; Zimmermann, R. Monoglyceride lipase deficiency causes desensitization of intestinal cannabinoid receptor type 1 and increased colonic mu-opioid receptor sensitivity. *British Journal of Pharmacology* **2015,** 172, 4419-4429.
50. Piomelli, D. More surprises lying ahead. The endocannabinoids keep us guessing. *Neuropharmacology* **2014,** 76 Pt B, 228-234.

51. Fowler, C. J.; Naidu, P. S.; Lichtman, A.; Onnis, V. The case for the development of novel analgesic agents targeting both fatty acid amide hydrolase and either cyclooxygenase or TRPV1. *British Journal of Pharmacology* **2009,** 156, 412-419.
52. Jung, K. M.; Astarita, G.; Zhu, C.; Wallace, M.; Mackie, K.; Piomelli, D. A key role for diacylglycerol lipase-alpha in metabotropic glutamate receptor-dependent endocannabinoid mobilization. *Molecular Pharmacology* **2007,** 72, 612-621.
53. Shonesy, B. C.; Wang, X.; Rose, K. L.; Ramikie, T. S.; Cavener, V. S.; Rentz, T.; Baucum, A. J., 2nd; Jalan-Sakrikar, N.; Mackie, K.; Winder, D. G.; Patel, S.; Colbran, R. J. CaMKII regulates diacylglycerol lipase-alpha and striatal endocannabinoid signaling. *Nature Neuroscience* **2013,** 16, 456-463.
54. Yuan, S.; Burrell, B. D. Endocannabinoid-dependent long-term depression in a nociceptive synapse requires coordinated presynaptic and postsynaptic transcription and translation. *The Journal of Neuroscience : the official Journal of the Society for Neuroscience* **2013,** 33, 4349-4358.
55. Bingol, B.; Sheng, M. Deconstruction for reconstruction: the role of proteolysis in neural plasticity and disease. *Neuron* **2011,** 69, 22-32.
56. Maccarrone, M.; Rossi, S.; Bari, M.; De Chiara, V.; Fezza, F.; Musella, A.; Gasperi, V.; Prosperetti, C.; Bernardi, G.; Finazzi-Agro, A.; Cravatt, B. F.; Centonze, D. Anandamide inhibits metabolism and physiological actions of 2-arachidonoylglycerol in the striatum. *Nature Neuroscience* **2008,** 11, 152-159.
57. Choi, S. H.; Langenbach, R.; Bosetti, F. Genetic deletion or pharmacological inhibition of cyclooxygenase-1 attenuate lipopolysaccharide-induced inflammatory response and brain injury. *FASEB Journal : official publication of the Federation of American Societies for Experimental Biology* **2008,** 22, 1491-1501.
58. Viader, A.; Ogasawara, D.; Joslyn, C. M.; Sanchez-Alavez, M.; Mori, S.; Nguyen, W.; Conti, B.; Cravatt, B. F. A chemoproteomic atlas of brain serine hydrolases identifies cell type-specific pathways regualting neuroinflammation.eLife **2016,** 5, e12345.
59. Kirilly, E.; Gonda, X.; Bagdy, G. CB1 receptor antagonists: new discoveries leading to new perspectives. *Acta Physiologica* **2012,** 205, 41-60.
60. Busquets-Garcia, A.; Gomis-Gonzalez, M.; Guegan, T.; Agustin-Pavon, C.; Pastor, A.; Mato, S.; Perez-Samartin, A.; Matute, C.; de la Torre, R.; Dierssen, M.; Maldonado, R.; Ozaita, A. Targeting the endocannabinoid system in the treatment of fragile X syndrome. *Nature Medicine* **2013,** 19, 603-607.
61. Bashashati, M.; Nasser, Y.; Keenan, C. M.; Ho, W.; Piscitelli, F.; Nalli, M.; Mackie, K.; Storr, M. A.; Di Marzo, V.; Sharkey, K. A. Inhibiting endocannabinoid biosynthesis: a novel approach to the treatment of constipation. *British Journal of Pharmacology* **2015,** 172, 3099-3111.
62. Oleson, E. B.; Beckert, M. V.; Morra, J. T.; Lansink, C. S.; Cachope, R.; Abdullah, R. A.; Loriaux, A. L.; Schetters, D.; Pattij, T.; Roitman, M. F.; Lichtman, A. H.; Cheer, J. F. Endocannabinoids shape accumbal encoding of cue-motivated behavior via CB1 receptor activation in the ventral tegmentum. *Neuron* **2012,** 73, 360-373.
63. Verdoes, M.; Florea, B. I.; Hillaert, U.; Willems, L. I.; van der Linden, W. A.; Sae-Heng, M.; Filippov, D. V.; Kisseley, A. F.; van der Marel, G. A.; Overkleeft, H. S. Azido-BODIPY acid reveals quantitative Staudinger-Bertozzi ligation in two-step activity-based proteasome profiling. *ChemBioChem* **2008,** 9, 1735-1738.

64. Liu, Y.; Patricelli, M. P.; Cravatt, B. F. Activity-based protein profiling: the serine hydrolases. *Proceedings of the National Academy of Sciences of the United States of America* **1999,** 96, 14694-14699.
65. Kidd, D.; Liu, Y.; Cravatt, B. F. Profiling serine hydrolase activities in complex proteomes. *Biochemistry* **2001,** 40, 4005-4015.
66. Patricelli, M. P.; Giang, D. K.; Stamp, L. M.; Burbaum, J. J. Direct visualization of serine hydrolase activities in complex proteomes using fluorescent active site-directed probes. *Proteomics* **2001,** 1, 1067-1071.
67. Hsu, K.-L. L.; Tsuboi, K.; Adibekian, A.; Pugh, H.; Masuda, K.; Cravatt, B. F. DAGLβ inhibition perturbs a lipid network involved in macrophage inflammatory responses. *Nature Chemical Biology* **2012,** 8, 999-1007.
68. Baggelaar, M. P.; Janssen, F. J.; van Esbroeck, A. C.; den Dulk, H.; Allarà, M.; Hoogendoorn, S.; McGuire, R.; Florea, B. I.; Meeuwenoord, N.; van den Elst, H.; van der Marel, G. A.; Brouwer, J.; Di Marzo, V.; Overkleeft, H. S.; van der Stelt, M. Development of an activity-based probe and in silico design reveal highly selective inhibitors for diacylglycerol lipase-α in brain. *Angewandte Chemie International Edition,* **2013,** 52, 12081-12085.
69. Janssen, F. J.; Deng, H.; Baggelaar, M. P.; Allarà, M.; van der Wel, T.; den Dulk, H.; Ligresti, A.; van Esbroeck, A. C.; McGuire, R.; Di Marzo, V.; Overkleeft, H. S.; van der Stelt, M. Discovery of glycine sulfonamides as dual inhibitors of sn-1-diacylglycerol lipase α and α/β-hydrolase domain 6. *Journal of Medicinal Chemistry* **2014,** 57, 6610-6622.
70. van der Wel, T.; Janssen, F. J.; Baggelaar, M. P.; Deng, H.; den Dulk, H.; Overkleeft, H. S.; van der Stelt, M. A natural substrate-based fluorescence assay for inhibitor screening on diacylglycerol lipase α. *Journal of Lipid Research* **2015,** 56, 927-935.
71. Bachovchin, D. A.; Ji, T.; Li, W.; Simon, G. M.; Blankman, J. L.; Adibekian, A.; Hoover, H.; Niessen, S.; Cravatt, B. F. Superfamily-wide portrait of serine hydrolase inhibition achieved by library-versus-library screening. *Proceedings of the National Academy of Sciences of the United States of America* **2010,** 107, 20941-20946.
72. Alexander, J. P.; Cravatt, B. F. Mechanism of carbamate inactivation of FAAH: implications for the design of covalent inhibitors and in vivo functional probes for enzymes. *Chemistry & Biology* **2005,** 12, 1179-1187.
73. Nomura, D. K.; Morrison, B. E.; Blankman, J. L.; Long, J. Z.; Kinsey, S. G.; Marcondes, M. C.; Ward, A. M.; Hahn, Y. K.; Lichtman, A. H.; Conti, B.; Cravatt, B. F. Endocannabinoid hydrolysis generates brain prostaglandins that promote neuroinflammation. *Science* **2011,** 334, 809-813.
74. Hyeon-Cheol, L.; Gabriel, M. S.; Benjamin, F. C. ABHD4 Regulates multiple classes of N-acyl phospholipids in the mammalian central nervous system. *Biochemistry* **2015**.
75. Inloes, J. M.; Hsu, K.-L. L.; Dix, M. M.; Viader, A.; Masuda, K.; Takei, T.; Wood, M. R.; Cravatt, B. F. The hereditary spastic paraplegia-related enzyme DDHD2 is a principal brain triglyceride lipase. *Proceedings of the National Academy of Sciences of the United States of America* **2014,** 111, 14924-14929.
76. Kamat, S. S.; Camara, K.; Parsons, W. H.; Chen, D.-H. H.; Dix, M. M.; Bird, T. D.; Howell, A. R.; Cravatt, B. F. Immunomodulatory lysophosphatidylserines are regulated by ABHD16A and ABHD12 interplay. *Nature Chemical Biology* **2015,** 11, 164-171.

77. Martin, B. R.; Wang, C.; Adibekian, A.; Tully, S. E.; Cravatt, B. F. Global profiling of dynamic protein palmitoylation. *Nature Methods* **2012,** 9, 84-89.
78. Hulce, J. J.; Cognetta, A. B.; Niphakis, M. J.; Tully, S. E.; Cravatt, B. F. Proteome-wide mapping of cholesterol-interacting proteins in mammalian cells. *Nature Methods* **2013,** 10, 259-264.
79. Washburn, M. P.; Wolters, D.; Yates, J. R. Large-scale analysis of the yeast proteome by multidimensional protein identification technology. *Nature Biotechnology* **2001,** 19, 242-247.
80. Weerapana, E.; Wang, C.; Simon, G. M.; Richter, F.; Khare, S.; Dillon, M. B.; Bachovchin, D. A.; Mowen, K.; Baker, D.; Cravatt, B. F. Quantitative reactivity profiling predicts functional cysteines in proteomes. *Nature* **2010,** 468, 790-795.
81. Pan, B.; Wang, W.; Long, J. Z.; Sun, D.; Hillard, C. J.; Cravatt, B. F.; Liu, Q.-s. S. Blockade of 2-arachidonoylglycerol hydrolysis by selective monoacylglycerol lipase inhibitor 4-nitrophenyl 4-(dibenzo[d][1,3]dioxol-5-yl(hydroxy)methyl)piperidine-1-carboxylate (JZL184) Enhances retrograde endocannabinoid signaling. *The Journal of Pharmacology and Experimental Therapeutics* **2009,** 331, 591-597.
82. Zhong, P.; Pan, B.; Gao, X.-p. P.; Blankman, J. L.; Cravatt, B. F.; Liu, Q.-s. S. Genetic deletion of monoacylglycerol lipase alters endocannabinoid-mediated retrograde synaptic depression in the cerebellum. *The Journal of Physiology* **2011,** 589, 4847-4855.
83. Kreitzer, A. C.; Regehr, W. G. Retrograde inhibition of presynaptic calcium influx by endogenous cannabinoids at excitatory synapses onto Purkinje cells. *Neuron* **2001,** 29, 717-727.
84. Bruno, C.; Manuel, S.-A.; Raphaelle, W.-S.; Maria Concetta, M.; Jacinta, L.; Sara, B.; Veronique, F.; Salvador, H.-R.; Steven, H.; Eric, P. Z.; Luis de, L.; Tamas, B. Transgenic mice with a reduced core body temperature have an increased life span. *Science* **2006**.
85. Eric, P. Z.; Manuel, S.-A.; Shuei, S.; Molly, B.; Rosette, F.; Tamas, B.; Bruno, C. Interleukin-18 controls energy homeostasis by suppressing appetite and feed efficiency. *Proceedings of the National Academy of Sciences* **2007**.
86. Manuel, S.-A.; Izabella, K.; Sara, E. B.; Iustin, V. T.; Christopher, N. D.; Bruno, C.; Tamas, B. Night eating and obesity in the EP3R-deficient mouse. *Proceedings of the National Academy of Sciences* **2007**.
87. Manuel, S.-A.; Iustin, V. T.; Olivia, O.; Kayo, M.; Jean, S.; Jeffrey, D.; Kristina, H. H.; Izabella, K.; Joe, K.; Luis, F. G.; Hartmuth, K.; James, S.; Jeanine, J.; Kevin, M.; Peter, B.; John, R. H.; James, E.; Bruno, C.; Tamas, B. Insulin Causes Hyperthermia by Direct Inhibition of Warm-Sensitive Neurons. *Diabetes* **2010**.
88. Zweemer, A. J.; Nederpelt, I.; Vrieling, H.; Hafith, S.; Doornbos, M. L.; de Vries, H.; Abt, J.; Gross, R.; Stamos, D.; Saunders, J.; Smit, M. J.; Ijzerman, A. P.; Heitman, L. H. Multiple binding sites for small-molecule antagonists at the CC chemokine receptor 2. *Molecular pharmacology* **2013,** 84, 551-561.